Bursting in a model with delay for networks of neurons

Inaugural-Dissertation

zur

Erlangung des Doktorgrades

der Mathematisch-Naturwissenschaftlichen Fakultät

der Universität zu Köln

vorgelegt von

Annette Gail

aus Haiger

2004

Berichterstatter: Prof. Dr. Tassilo Küpper
Prof. Dr. Dietrich Stauffer

Tag der mündlichen Prüfung: 13. Juli 2004

Contents

Chapter 1

Introduction

Neurons display three different types of dynamics: Stationary behaviour and oscillations in the form of bursting and spiking. Bursting is characterised by oscillations that are interrupted by quasistationary behaviour whereas spiking consists of continous oscillations. Bursting is linked to many neural processes. For example sleep oscillations in thalamocortical systems display bursting [33] as well as respiratory pacemaker neurons [3]. The responses of cells in the visual cortex of the cat to intracellular injection of current pulses [30] show classes of characteristic oscillatory behaviour (see figure 1.1). Four main classes of oscillations are observed there: Regular spiking, fast spiking, chattering and intrinsic bursting. Chattering cells consist also of bursts, they generate repetitive bursting of thin action potentials.
In this thesis the phenomenon of bursting in a mathematical model for neurons is investigated by connecting it with the bifurcation properties of the model. This leads to a better understanding of the underlying mechanisms of bursting and gives new criteria for the occurence of bursting in dependence on parameters of the neuron model used.

1.1 Neuron models

Mathematical models for neuron potentials are often based on the Hodgkin-Huxley model [23, 25, 11] which was developed to describe the action potentials in the squid giant axon. The description of the transmission of electrical pulses along a nerve membrane relies on the balance of a current that passes a resistance and the change of the membrane potential v of the neuron.

$$C_m \frac{dv}{dt} + I_{ion} = 0 \tag{1.1}$$

The membrane potential v is the difference between internal and external voltage and the ion current depends on the specific membrane resistance: $I_{ion} = v/R$.

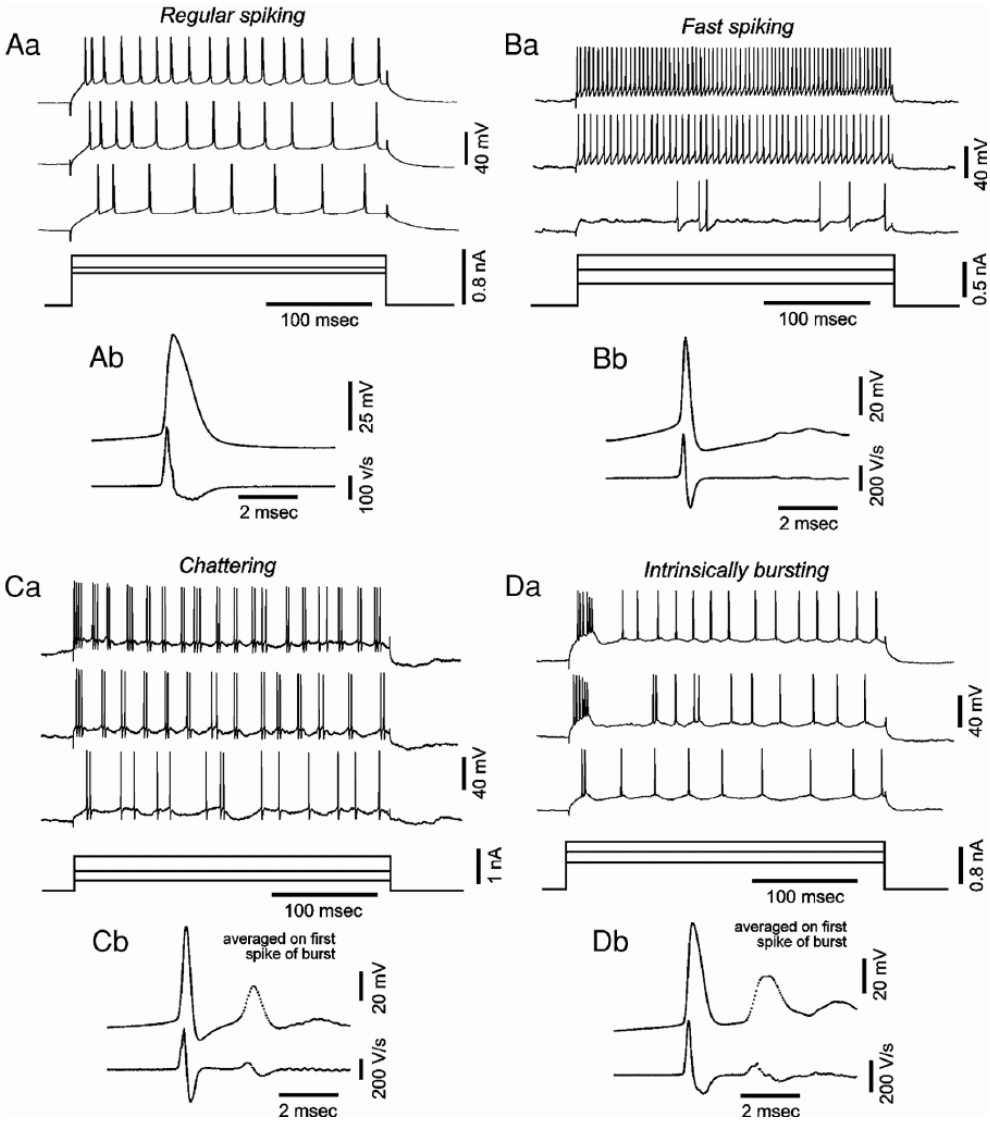

Figure 1.1: Examples of action potential responses of cats cortical neurons (picture taken from [30]).

The Hodgkin-Huxley model consists of an equation for the membrane potential v of the neuron that depends on several ionic currents (sodium ion currents, potassium ion currents and leak currents) and auxiliary equations modelling the gating of ion channels. We refer to appendix A for the description of the Hodgkin-Huxley equations.
FitzHugh and Nagumo developed a system that has similar qualitative properties than the four-dimensional Hodgkin-Huxley model but it is in contrast only two-dimensional [12, 29]. FitzHugh's system gives accurate descriptions of an action potential only for the initial stage but since its equations are simpler it is an appropriate ansatz for numerical and analytical investigations of neurons. A general version of the FitzHugh-Nagumo model which is described in [25] is system

$$\begin{aligned} \epsilon\frac{dv}{dt} &= f_1(v,w) + I, \\ \frac{dw}{dt} &= f_2(v,w) \end{aligned} \tag{1.2}$$

where v denotes the membrane potential, w is considered as auxiliary variable, I is a current that is generated by synapses and by external signals and ϵ being a small constant parameter. Here the function $f_1(v,w)$ is a cubic polynomial and $f_2(v,w)$ is a linear function. In this thesis the following special variant of FitzHugh-Nagumos system is employed which is described in detail in [14, 17]:

$$\begin{aligned} \dot{v}(t) &= c(w(t) + v(t) - \frac{1}{3}v^3(t)) + u, \\ \dot{w}(t) &= (a - v(t) - bw(t))/c. \end{aligned} \tag{1.3}$$

Here, the external input to the system is replaced by the parameter u. a, b, c are constant parameters. In [14] the FitzHugh-Nagumo system (1.3) is regarded as nonlinear oscillator that generates the outgoing signal or membrane potential of a neuron. All incoming signals of a neuron that are collected at the synapses are commuted into the total postsynaptic potential u. A network equation in [14] models the cumulation of the incoming presynaptic potentials v and the generation of the total postsynaptic potential u.

$$\tau\dot{u}(t) = -u(t) + qg(v(t-T)) + e \tag{1.4}$$

The parameter τ characterises the relaxation time of the postsynaptic potential. In biology three main classes of postsynaptic potentials are distinguished: fast, slow and late slow postsynaptic potentials. They differ from each other in their relaxation time. A more detailed description of these temporal postsynaptic dynamics is given in chapter 6 of this thesis. Coupling between neurons occurs at the synapses of a neuron. Synapses that strengthen the incoming presynaptic potential are called excitatory synapses and are presented in (1.4) by positive

coupling constants q. Inhibitory coupling weakens or represses presynaptic potentials and are denoted in the network equation by negative values of q. Taking into account the propagation time of neural signals along the axon and the dendrites a time delay T is appended. The relation between pre- and postsynaptic potential is given by the nonlinear sigmoidal transfer function g.

$$g(v(t-T)) = \frac{1}{1+\exp(-4v(t-T))} \tag{1.5}$$

Further external signals are considered with the variable e.
Pulling together the network equation and the FitzHugh-Nagumo oscillator we acquire completingly a mathematical model for neural cells which is applied in this thesis.

$$\begin{aligned} \tau\dot{u}(t) &= -u(t) + qg(v(t-T)) + e, \\ \dot{v}(t) &= c(w(t) + v(t) - \frac{1}{3}v^3(t)) + u(t), \\ \dot{w}(t) &= (a - v(t) - bw(t))/c \end{aligned} \tag{1.6}$$

General analytical and numerical investigations of the model as well as applications in the range of epileptiform activity can be read in [14, 13, 21, 20].
In terms of biology the neuron model is extended to an m-dimensional system displaying a network of coupled cells.

$$\begin{aligned} \tau_i\dot{u}_i(t) &= -u_i(t) + \sum_{k=1}^{m} q_{ik}g(v_k(t-T_{ik})) + e_i, \\ \dot{v}_i(t) &= c(w_i(t) + v_i(t) - \frac{1}{3}v_i^3(t)) + u_i, \\ \dot{w}_i(t) &= (a - v_i(t) - bw_i(t))/c. \end{aligned}$$

Figure 1.2 shows a sketch of the processes that take place during signal transmission. Incoming signals $v_k(t-T_{ik})$ are collected at the synapses. Subsequently the total postsynaptic potential $u_i(t)$ is generated and propagates to the axon hillock of the neuron. At the axon hillock the postsynaptic potential can evoke an outgoing membrane potential v_i if it exceeds a certain threshold.
System (1.6) exhibits two different oscillation modes: bursting and spiking that are controlled primarily by the parameters e and q. The FitzHugh-Nagumo oscillator (1.3) can be considered as the fast subsystem of the whole model. The oscillatory dynamics of the fast subsystem alone consists only of spikes. In combination with a slow subsystem that is in our model the network equation (1.4) the whole system is also able to oscillate in the bursting mode. Bursting in the context of slow-fast systems has been investigated for other neural models, see for example [32].

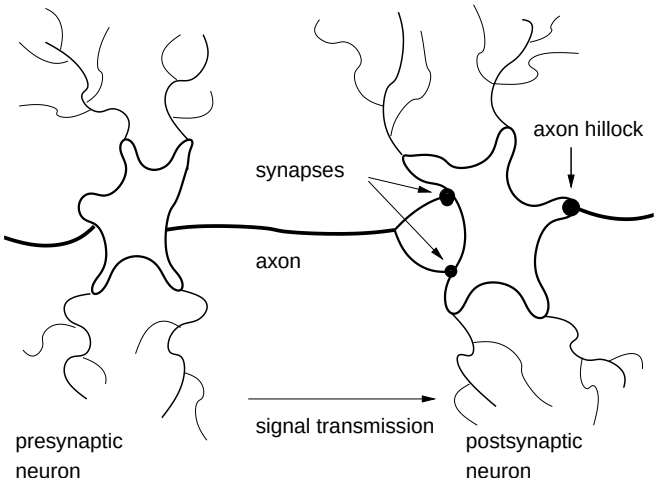

Figure 1.2: Sketch of two coupled neurons displaying signal transmission.

1.2 Outline of the thesis

It is the intention of the thesis to investigate the bursting mode of the neural system (1.6). This will lead to a better understanding of the underlying mechanisms of bursting and in that way new criteria for the occurence of bursting in dependence on important parameters of our neuron model are developed.
For this purpose bifurcation properties of the neuron model are analysed and are connected with the bursting properties of the model. The most important bifurcation parameter of the system is the external signal e. Former investigations of the model [14, 13, 21] have already shown that the onset of oscillations can be controlled by the parameter e. Further a range of e had been determined empirically for which bursting in a single neuron as well as in networks of neurons occurs. The task of this thesis is to specify the appearance of bursting in detail and to give criteria for the occurence of bursting that are directly taken from the bifurcation analysis of the model.
Since the neuron model is three dimensional, nonlinear and contains a time delay it is not possible to obtain a full bifurcation analysis by using analytical methods. We therefore approach the investigation of the bifurcation properties of the system with respect to the parameter e from three sides and combine the obtained results in order to explain bursting behaviour.

In chapter 2 the neural system (1.6) is examined for the limiting case of infinite delay T. An iterated map can then be derived from the equations of the system. The iterated map is investigated with analytical and numerical methods. It turns out that the map possesses a bifurcation to periodic solutions. The critical values of e that correspond to the bifurcation points of the map are determined. Further

the type of the bifurcation is classified and the stability of the periodic region of the map is determined.
Chapter 3 contains a bifurcation analysis of the neuron model based on the transition of stable stationary solutions to unstable stationary solutions. The obtained transition points are potential Hopf points of the system. At a Hopf point there occurs a bifurcation to periodic solutions. The transition points are determined for finite and infinite delay T, in both cases with respect to the parameters e and q of the model. In addition, the system is analysed for the limiting case of infinite time constant τ.
In chapter 4 a numerical bifurcation analysis of the neural system (1.6) is carried out. With the help of the Matlab package DDE-BIFTOOL [9] that allows the numerical analysis of retarded differential equations the Hopf points of the system were detected. Branches of periodic solutions that emanate from the Hopf points are followed and their stability is determined with the help of Floquet multipliers. The numerical bifurcation analysis yields a bifurcation diagram of the variable v with respect to the bifurcation parameter e. This result is the first bifurcation diagram that was obtained for the full, time delayed neuron model. Existing publications on the neuron model only deal with the bifurcation properties of the underlying FitzHugh-Nagumo system.
The results of the numerical bifurcation analysis are compared with the results of the iterated map and those of the analysis of the transition points in chapter 5. With the help of the numerical bifurcation analysis the potential Hopf points of the analysis of the loss of stability can be determined to be real Hopf bifurcation points. In addition, numerical simulations of the solutions of the neural system are related to the results of the analysis of the iterated map and to examples of the numerical bifurcation analysis. Pulling these results together allows for a deeper understanding of the origin of bursting. We succeed in giving criteria for the occurence of bursting that are directly related to the bifurcation properties of the model.
An application of the bursting phenomena of our model is presented in chapter 6. By means of enlarging the number of network equations in the neuron model it is possible to model different classes of postsynaptic potentials that occur in nature. Due to the interaction of multiple time scales the appearance of burst multiplets is observed in numerical simulations. A reduction of the multiple time scale model to a three time scale model is given and the phenomenon of burst multiplets is described on the basis of this reduced model. The burst multiplets are finally related to experimental data coming from respiratory research.
An outlook of further aspects of the neuron model whose analysis seems to be rewarding is given in chapter 7. A discussion and summary of the attained results concludes this thesis.

Chapter 2

The iterated map

It is one aim of this work to find criteria for the occurence of bursting which are based directly on the mathematical properties of the neuron model.
The phenomenon of bursting in networks of neurons which are modelled by the following system (2.1) has been investigated numerically in [20] both for small and large networks.

$$\begin{aligned} \tau\dot{u}(t) &= -u(t) + qg(v(t-T)) + e, \\ \dot{v}(t) &= c(w(t) + v(t) - \frac{1}{3}v^3(t)) + u(t), \\ \dot{w}(t) &= (a - v(t) - bw(t))/c. \end{aligned} \tag{2.1}$$

For appropriate parameters q and e and for $\tau \gg \frac{1}{c}$ system (2.1) displays bursting [14]. Figure 2.1 shows that the dynamics of v is characterised during bursting by an alternation between a quasistationary state and a state of repetitive firing. If the total postsynaptic potential enters the oscillation interval I_{osc} (indicated by dotted lines in figure (2.1)) of the FitzHugh-Nagumo oscillator the membrane potential v starts to oscillate. Due to the delayed incoupling of v with a negative coupling term the postsynaptic potential is pushed outside the oscillation interval and the oscillation is terminated. After relaxation u returns into the oscillation interval because of the quasistationary behaviour of v that pushes u. The cycle starts again and a further burst is generated.
The most important bifurcation parameter of the system is the external signal e. Numerical simulations have shown that the neural system (2.1) displays bursting only for a small regime of e. An investigation of the mathematical model with analytical and numerical methods will give criteria for the dependence of bursting on the bifurcation parameter e.
Especially in this chapter the bifurcation behaviour of the neuron model is investigated for infinite delay T by deriving an iterated map for the model. After an introduction of different types of bifurcations of iterated maps a bifurcation analysis is performed which yields the type of bifurcation of the iterated map as well

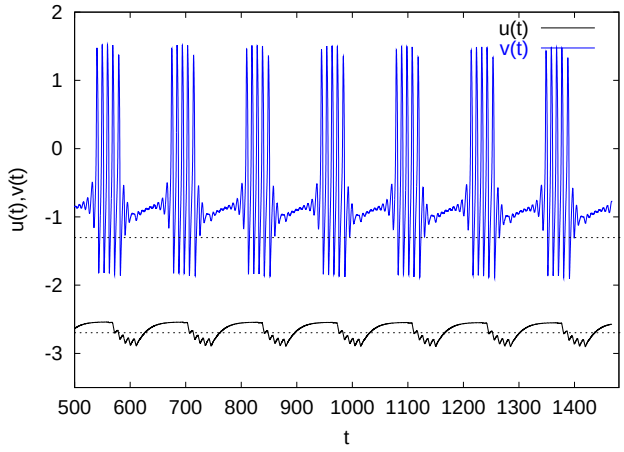

Figure 2.1: Bursting of the single neuron. The oscillation interval of the FitzHugh-Nagumo subsystem is indicated by the dotted lines. The simulation was performed for $(a, b, c, q, \tau, T, e) = (0.9,\ 0.9,\ 2.0,\ -1.0,\ 20,\ 30,\ -2.5)$.

as its stability properties. Finally the parameter values e for which bifurcations occur are determined.

2.1 Derivation of the iterated map

Investigating the oscillation properties of the neural system (2.1) with respect to the bifurcation parameter is a difficult task because the phase space of retarded differential equations is infinite dimensional and no complete bifurcation theory exists in this case. The limiting case of infinite delay simplifies our neural system and so it is possible to examine the dynamics of system. First a variable transformation has to be accomplished in order to simplify calculating the limit. The new variables are given by
$s := \frac{t}{T}$, $U(s) := u(Ts)$, $V(s) := v(Ts)$ and $W(s) := w(Ts)$.
Under this transformation the system (1.6) becomes

$$\begin{aligned} \frac{\tau}{T}\frac{dU(s)}{ds} &= -U(s) + qg(V(s-1)) + e, \\ \frac{1}{T}\frac{dV(s)}{ds} &= c(W(s) + V(s) - \frac{1}{3}V^3(s)) + U(s), \\ \frac{1}{T}\frac{dW(s)}{ds} &= (a - V(s) - bW(s))/c. \end{aligned} \tag{2.2}$$

Carrying out the limit $T \to \infty$ we obtain a difference-algebraic system

$$\begin{aligned} 0 &= -U(s) + qg(V(s-1)) + e, \\ 0 &= c(W(s) + V(s) - \frac{1}{3}V^3(s)) + U(s), \\ 0 &= (a - V(s) - bW(s))/c. \end{aligned} \tag{2.3}$$

With the auxiliary function $H(V(s))$

$$H(V(s)) := c(\frac{1}{3}V^3(s) + V(s)(\frac{1}{b} - 1) - \frac{a}{b}) = U(s) \tag{2.4}$$

a scalar iterated map is deduced from (2.3). The U-representation of the the map is given by

$$U_{n+1} = qg(H^{-1}(U_n)) + e. \tag{2.5}$$

The explicit formula of the inverse $H^{-1}(U(s))$ of the auxiliary function is given in appendix B. For the V-representation we obtain

$$\frac{c}{3}V_{n+1}^3 - c(1 - \frac{1}{b})V_{n+1} = qg(V_n) + \frac{ac}{b} + e. \tag{2.6}$$

Since we are considering real variables we always take the real roots when we solve the polynomials of third order.

2.2 Bifurcation of the iterated map

A bifurcation analysis of the iterated map is obtained in the following. In addition the type of bifurcation is determined by a combination of analytical and numerical methods.
Computing the bifurcation diagram of the scaled iterated map in dependence on the parameter e shows the existence of an area of periodic solutions.
The iterates of the map represent the two types of dynamics of the system. Iterates for values of e that correspond to stationary solutions of the iterated map are shown in figure 2.3 as well as iterates for e lying in the periodic region of the iterated map. The numerical computed bifurcation diagrams of the iterated map, see figure 2.2, show that a period doubling bifurcation occurs and that the transition to the periodic solutions is supercritical. Properties of the period doubling bifurcation, which is also called flip bifurcation or subharmonic bifurcation are shown in the next subsection. Subsequently, our iterated map is investigated with respect to the properties of the flip bifurcation to verify its bifurcation type.

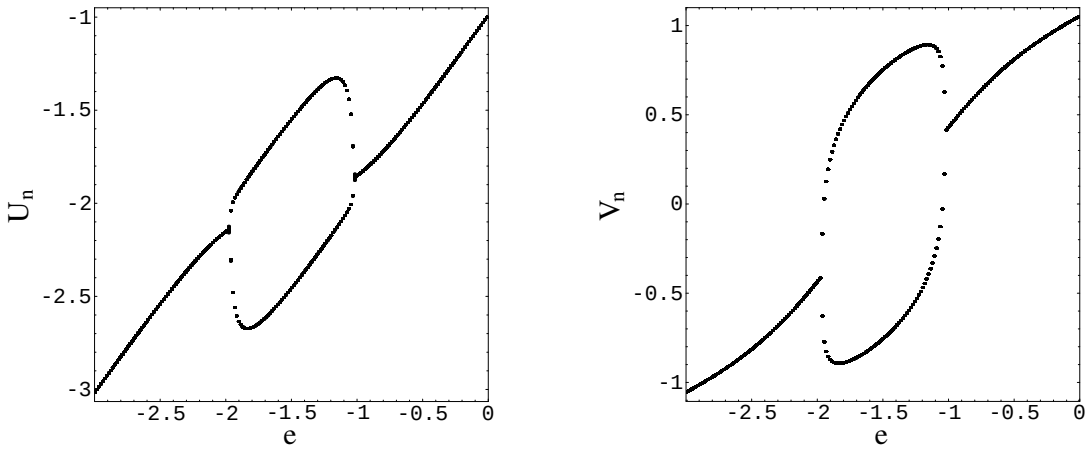

Figure 2.2: Bifurcation diagrams of the iterated map with respect to the parameter e. The left figure shows the bifurcation diagram for U and the right figure displays the dependence of V on e. The parameters of the computation were $a = b = 0.9$, $c = 2.0$ and $q = -1.0$.

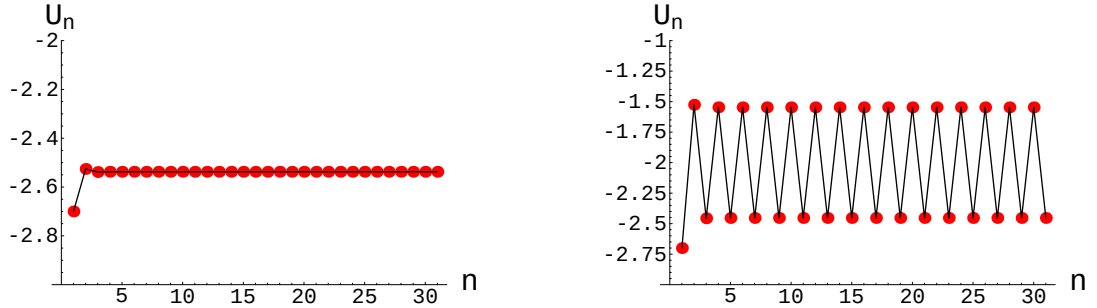

Figure 2.3: Iterates of the scalar map. Left: Stationary solution. Iterates for $e = -2.5$. Right: Periodic solution. Iterates for $e = -1.5$.

2.2.1 Flip bifurcation

Discrete dynamical systems show three main classes of one-parameter bifurcations of fixed points: the saddle-node bifurcation, the flip bifurcation and the Neimark-Sacker bifurcation. Scalar systems have the lowest possible dimension for the occurence of saddle-node and flip bifurcations. Neimark-Sacker bifurcations appear only in planar systems and higher dimensional systems. For a detailed description of iterated maps see [36, 28, 18].
Consider a discrete dynamical system depending on the parameter μ

$$x \mapsto f(x, \mu), \qquad x \in \mathbb{R}^n, \quad \mu \in \mathbb{R}^n \tag{2.7}$$

where f is C^r. Suppose (2.7) has a fixed point at $(x, \mu) = (x_0, \mu_0)$.

Definition 2.1 *A fixed point (x_0, μ_0) of $f : \mathbb{R}^n \to \mathbb{R}^n$ is called hyperbolic if $D_x f(x_0, \mu_0)$ has no eigenvalues on the unit circle. $D_x f(x_0, \mu_0)$ is the Jacobian matrix at the fixed point.*

Bifurcations of maps only occur if the hyperbolicity condition is violated. There are three ways in which a fixed point of a map can be nonhyperbolic.

Definition 2.2 *Saddle-node bifurcation: The linearised map $D_x f(x_0, \mu_0)$ has a single eigenvalue equal to 1 and the remaining n-1 eigenvalues have moduli not equal to 1.*
Flip bifurcation: The linearised map $D_x f(x_0, \mu_0)$ has a single eigenvalue equal to -1 and the remaining n-1 eigenvalues have moduli not equal to 1.
Neimark-Sacker (torus) bifurcation: The linearised map $D_x f(x_0, \mu_0)$ has a pair of complex conjugate eigenvalues having moduli 1 and the remaining n-2 eigenvalues have moduli not equal to 1.

Since we are considering a one dimensional iterated map the Neimark-Sacker bifurcation does not have any importance for the further considerations. The saddle-node bifurcation however can occur in the iterated map and we will go into this in the further course of the bifurcation analysis.
In the following the flip bifurcation is considered in its lowest possible dimension and we obtain a one dimensional iterated map.

$$x \mapsto f(x, \mu), \qquad x \in \mathbb{R}, \quad \mu \in \mathbb{R} \tag{2.8}$$

f is in this case C^3. In addition to the eigenvalue criterium it is sufficient for system (2.8) to satisfy the following two conditions that can be found in the book of Guckenheimer [16].

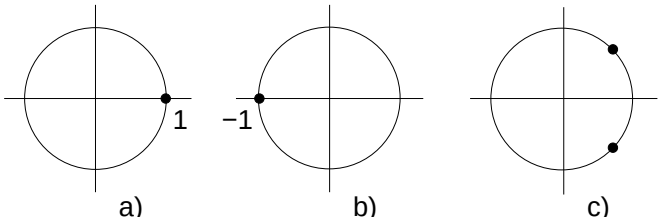

Figure 2.4: Eigenvalues on the unit circle of the complex plane corresponding to nonhyperbolicity: a) Saddle-node bifurcation, b) Flip bifurcation, c) Neimark-Sacker bifurcation.

Theorem 2.1 *Let $f : \mathbb{R} \to \mathbb{R}$ be a one-parameter family of mappings such that f_0 has a fixed point x_0 with eigenvalue -1. Assume*

$$(\frac{\partial f}{\partial \mu}\frac{\partial^2 f}{\partial x^2} + 2\frac{\partial^2 f}{\partial x \partial \mu}) = \frac{\partial f}{\partial \mu}\frac{\partial^2 f}{\partial x^2} - (\frac{\partial f}{\partial x} - 1)\frac{\partial^2 f}{\partial x \partial \mu} \neq 0 \quad at\ (x_0, \mu_0), \tag{F1}$$

$$a = (\frac{1}{2}(\frac{\partial^2 f}{\partial x^2})^2 + \frac{1}{3}(\frac{\partial^3 f}{\partial x^3})) \neq 0 \quad at\ (x_0, \mu_0). \tag{F2}$$

Then there is a smooth curve of fixed points of f passing through (x_0, μ_0), the stability of which changes at (x_0, μ_0). There is also a smooth curce γ passing through (x_0, μ_0) so that $\gamma - \{(x_0, \mu_0)\}$ is a union of hyperbolic period 2 orbits. The curve γ has quadratic tangency with the line $\mathbb{R} \times \{\mu_0\}$ at (x_0, μ_0).

$F1$ is the μ-derivative of f' along the curve of the fixed points and condition $F2$ determines the stability of the periodic orbits. A positive value of a is related to stable periodic orbits and if a is negative the periodic orbits are unstable. In addition $F2$ gives the direction of bifurcation of the periodic orbits: positive a correspond to supercritical bifurcations and negative a to subcritical bifurcations. Figure 2.5 shows a sketch of the two bifurcation directions.

2.2.2 Bifurcation analysis

Starting from the description of a general flip bifurcation in the last subsection now the flip bifurcation points of the scalar iterated map

$$U \mapsto q\,g(H^{-1}(U)) + e \tag{2.9}$$

are calculated. For the fixed points $\bar{U}$ of (2.9) we obtain

$$\bar{U} = q\,g(H^{-1}(\bar{U})) + e. \tag{2.10}$$

An example of numerically calculated fixed points of the V-map in dependence on the parameter e is given in figure 2.7. In the case of a saddle-node bifurcation

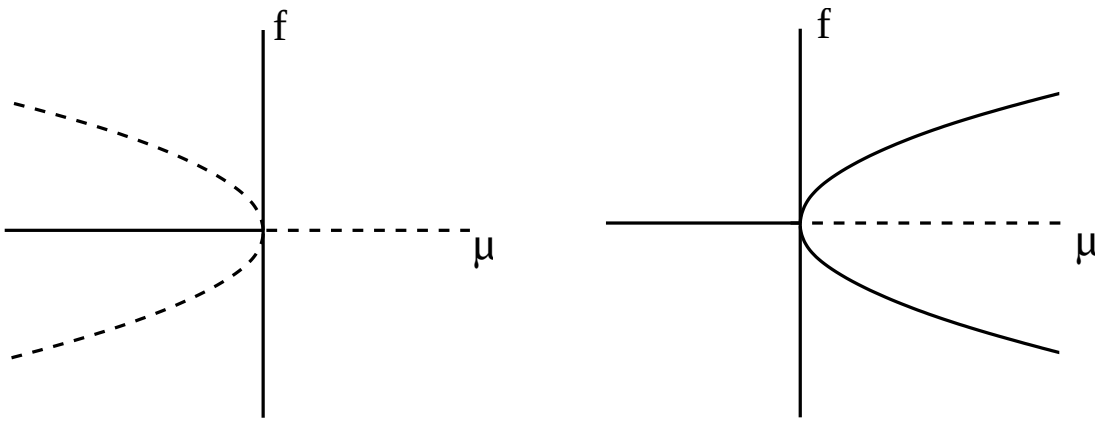

Figure 2.5: Sketch of bifurcation directions of the flip bifurcation. Left: Subcritical bifurcation. Right: Supercritical bifurcation. Solid lines represent stable solutions and dashed lines represent unstable solutions.

the eigenvalue of the linearisation of (2.9) at the fixed point is equal to 1. In order to compare the results of the iterated map with results of the following chapters the further analysis is restricted to a special set of parameters that leads to a flip bifurcation of the iterated map. Therefore we will not study the saddle-node bifurcation subsequently.
The linearisation of (2.9) at the fixed point is equal to -1 for flip bifurcations.

$$D(qg(H^{-1}(U)) + e) = -1. \tag{2.11}$$

This is equivalent to

$$q\ g'(H^{-1}(U))\ \frac{1}{H'(H^{-1}(U))} = -1. \tag{2.12}$$

We restrict the further analysis to the case $q = -1$ for which bifurcation diagrams were shown in figure 2.2 and obtain

$$g'(H^{-1}(U)) = H'(H^{-1}(U)). \tag{2.13}$$

Inserting the auxiliary function

$$H(x) := c(\frac{1}{3}x^3 + x(\frac{1}{b} - 1) - \frac{a}{b}) \tag{2.14}$$

into the equation above leads to

$$g'(H^{-1}(U)) = c\,((H^{-1}(U))^2 + \frac{1}{b} - 1). \tag{2.15}$$

The sigmoidal function

$$g(x) = \frac{1}{1 + \exp(-4x)} \tag{2.16}$$

has a maximal slope of 1. The derivative H' of the auxiliary function has a minimum at $x = 0$ since we are always considering positive c in our model. With the standard choice of $b = 0.9$ and $c = 2.0$ the minimum of H' at $x = 0$ has the value $\frac{2}{9}$. This implies that the derivatives of the function g and H have two points of intersection which is shown in figure 2.6. The two intersection points $H^{-1}(u_1)$

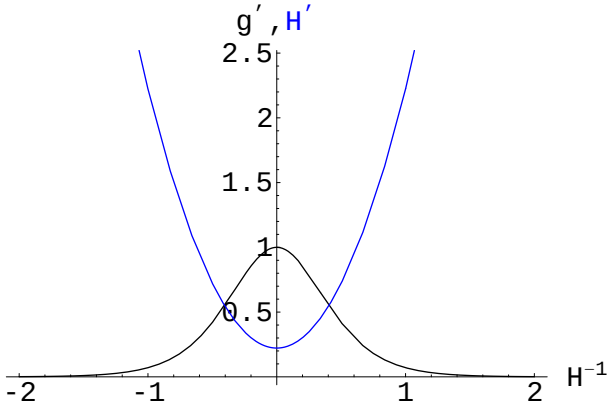

Figure 2.6: Intersections of the derivatives of g (shown in black) and H (drawn in blue) for the parameters $b = 0.9$ and $c = 2.0$.

and $H^{-1}(u_2)$ were calculated numerically, u_1 and u_2 were determined with the help of the inverse H^{-1} for the parameter values $(a, b, c, q) = (0.9,\ 0.9,\ 2.0,\ -1.0)$. Inserting this into the iterated map yields the two bifurcation points e_1 and e_2 of the flip bifurcation.

$$e_1^{flip} = -1.97 \qquad\qquad e_2^{flip} = -1.03 \tag{2.17}$$

The numerically calculated bifurcation diagrams for the same set of parameters are shown in figure (2.2). They are in total agreement with the bifurcation points e_1^{flip} and e_2^{flip} obtained in the previous calculation.
The bifurcation analysis of the iterated map is completed by calculating the conditions given in theorem (2.1). Computing condition $(F1)$ guarantees that a single curve of fixed points passes through (x_0, μ_0). Condition $(F2)$ gives information about the stability of the periodic orbit and the direction of the bifurcation of the periodic orbit. The two conditions were calculated using the V representation of the iterated map and the usual set of parameters $(a, b, c, q) = (0.9,\ 0.9,\ 2.0,\ -1.0)$. Evaluating both conditions leads to

$$\text{flip point 1}: \begin{cases} (F1) \ \text{ is positive at } \ (v_1^{flip}, e_1^{flip}), \\ \\ (F2) \ \text{ is positive at } \ (v_1^{flip}, e_1^{flip}) \end{cases} \tag{2.18}$$

for the first flip point and for the second flip point there holds

$$\text{flip point } 2: \begin{cases} (F1) \text{ is positive at } (v_2^{flip}, e_2^{flip}), \\ \\ (F2) \text{ is positive at } (v_2^{flip}, e_2^{flip}). \end{cases} \tag{2.19}$$

The calculation of $(F1)$ and $(F2)$ have shown that for both flip points the bifurcating periodic solutions are stable and that the direction of the bifurcating periodic orbit is supercritical.

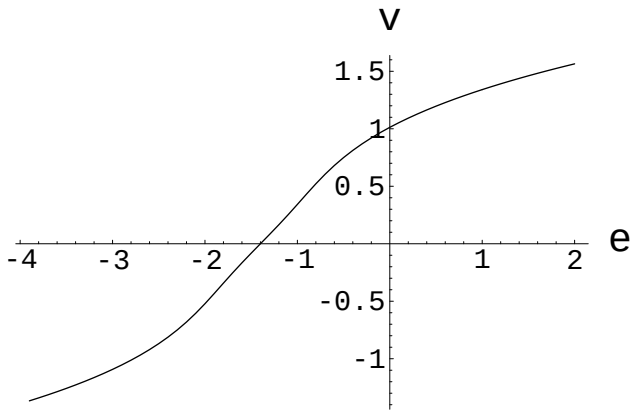

Figure 2.7: Curve of fixed points of V with respect to the parameter e. The calculation was performed for $(a, b, c, q) = (0.9,\ 0.9,\ 2.0,\ -1.0)$.

Chapter 3

Bifurcation properties of the neural system

In the previous chapter the bifurcation points for infinite delay were calculated. The objective of this chapter however is the calculation of bifurcation points of the neural system for finite delay.
The direct calculation of Hopf points is difficult for the system (3.1) because it consists of three coupled nonlinear differential equations with delay. Nevertheless it is possible to examine the bifurcation behaviour of the neural system by studying the loss of stability of the stationary solutions. The latter facilitates to determine transition points between stationary and periodic behaviour. These transition points are potential Hopf points of the system

$$\begin{aligned} \tau\dot{u}(t) &= -u(t) + qg(v(t-T)) + e, \\ \dot{v}(t) &= c(w(t) + v(t) - \frac{1}{3}v^3(t)) + u(t), \\ \dot{w}(t) &= (a - v(t) - bw(t))/c. \end{aligned} \tag{3.1}$$

In the first two sections a review of results of the analysis of the neural system is given which yields the potential Hopf points in dependence on the parameter q for finite delay T. This review is taken from [14]. An analysis of the loss of stability of the neural system in the case of infinite delay T and infinite time constant τ is given in the subsequent sections.

3.1 Existence and uniqueness of stationary solutions

The solutions $(u, v, w) \in I\!R^3$ of system (3.1) are stationary in the case of

$$\begin{aligned} \tilde{H}(v) &:= \tfrac{c}{3}v^3 + c(\tfrac{1}{b} - 1)v - qg(v) = e + \tfrac{ac}{b} \\ u &= qg(v) + e \\ w &= \tfrac{a-v}{b}. \end{aligned} \tag{3.2}$$

The following lemma gives conditions for the existence and the uniqueness of the stationary solution. The lemma and the proof were taken from [14].

Lemma 3.1 *(Existence of stationary solutions)*
Assume $a, c > 0$ and $0 < b < 1$. Further we assume $g \in C^2(\mathbb{R}, \mathbb{R})$ is an increasing function satisfying $g''(v)v < 0$ for all $v \neq 0$.

1. *If $c(\frac{1}{b} - 1) \geq qg'(0)$ then for any $e \in \mathbb{R}$ equation (3.1) possesses a unique stationary solution.*

2. *If $c(\frac{1}{b} - 1) < qg'(0)$ then there exist e_1, $e_2 \in \mathbb{R}$ with $e_2 < e_1$ such that*
   (a) for $e \in (-\infty, e_2) \cup (e_1, +\infty)$ equation (3.1) has exactly one stationary solution,
   (b) for $e \in \{e_1, e_2\}$ equation (3.1) has exactly two stationary solutions,
   (c) for $e \in (e_2, e_1)$ equation (3.1) has exactly three stationary solutions.

Proof: Since

$$\lim_{v \to \pm\infty} \tilde{H}(v) = \pm\infty \ , \tag{3.3}$$

equation (3.1) has at least one stationary solution.
For $c(\frac{1}{b} - 1) \geq qg'(0)$ the function $\tilde{H}$ is strictly increasing. This provides the uniqueness of the stationary solution.
For $c(\frac{1}{b} - 1) < qg'(0)$ there are exactly two solutions v_{01} and v_{02} with $v_{01} < 0 < v_{02}$ of

$$\tilde{H}'(v) = cv^2 + c(\frac{1}{b} - 1) - qg'(v) = 0 \ , \tag{3.4}$$

such that $\tilde{H}$ is strictly increasing on $(-\infty, v_{01}]$ and $[v_{02}, +\infty)$, and strictly decreasing on $[v_{01}, v_{02}]$.
Setting

$$e_i := \tilde{H}(v_{0i}) - \frac{ac}{b} = (\frac{c}{3}v_{0i}^3 + c(\frac{1}{b} - 1)v_{0i}) - qg(v_{0i}) \ , \quad i = 1, 2 \ , \tag{3.5}$$

completes the proof. The dependence of e_i on the parameter q is shown in figure 3.1 which is plotted in the next section.

3.2 Stability of stationary solutions

The loss of stability of the stationary solutions is calculated in this section and conditions for the transition to oscillatory dynamics are given in dependence on the parameters q and e.
Let $(\bar{u}, \bar{v}, \bar{w}) \in \mathbb{R}^3$ be a stationary solution of the system (1.6). The linearisation of a delay equation system is given by the Fréchet-map in the Banach space.

$$DF(\bar{x}) = DF(\bar{x})\, x(t) + DF(\bar{x})\, x(t - T) \tag{3.6}$$

Applying this to our system yields

$$\begin{aligned} \tau\dot{u}(t) &= -u(t) + q\ g'(\bar{v})v(t-T), \\ \dot{v}(t) &= c\left(w(t) + (1-\bar{v}^2)v(t)\right) + u(t), \\ \dot{w}(t) &= \left(-v(t) - bw(t)\right)/c. \end{aligned} \tag{3.7}$$

To calculate the characteristic equation of system (3.7) we choose the following ansatz for the derivatives of the left side

$$X = (u(t), v(t), w(t))^T := e^{zt} \cdot \xi \tag{3.8}$$

Inserting this into the linearisation

$$\dot{X}(t) = AX(t) + BX(t-T) \tag{3.9}$$

with

$$A = \begin{pmatrix} -\frac{1}{\tau} & 0 & 0 \\ 1 & c(1-\bar{v}^2) & c \\ 0 & -\frac{1}{c} & -\frac{b}{c} \end{pmatrix} \quad \text{and} \quad B = \begin{pmatrix} 0 & \frac{1}{\tau}gg'(\bar{v}) & 0 \\ 0 & 0 & 0 \\ 0 & 0 & 0 \end{pmatrix} \tag{3.10}$$

gives the characteristic equation of the linearised system

$$\chi(z) = \det(z\mathbf{1} - A - Be^{-zT}) = 0 \tag{3.11}$$

which is equivalent to

$$\chi(z) = \det \begin{pmatrix} z + \frac{1}{\tau} & -\frac{e^{-zT}gg'(\bar{v})}{\tau} & 0 \\ -1 & z - c(1-\bar{v}^2) & -c \\ 0 & \frac{1}{c} & \frac{b}{c} + z \end{pmatrix}. \tag{3.12}$$

Evaluating the determinant gives the following expression for the characteristic equation

$$\chi(z) = p_3(z) - \frac{qg'(\bar{v})}{\tau}(z + \frac{b}{c})\exp(-zT) = 0 \tag{3.13}$$

where p_3 is a third order polynomial

$$p_3(z) = (z + \frac{1}{\tau})(z^2 - c(1 - \frac{b}{c^2} - \bar{v}^2)z + b(\bar{v}^2 + \frac{1}{b} - 1)). \tag{3.14}$$

For $z \neq -\frac{b}{c}$ the characteristic polynomial is equivalent to

$$q = \frac{\tau p_3(z)\exp(zT)}{(z + \frac{b}{c})g'(\bar{v})}. \tag{3.15}$$

$z = i\omega, \omega \in \mathbb{R}$ is a solution of (3.13) if and only if

$$q = \delta_r(\omega, \bar{v}) \tag{3.16}$$

and

$$\delta_i(\omega, \bar{v}) = 0, \tag{3.17}$$

where

$$\delta_r(\omega, \bar{v}) := \Re\left(\frac{\tau p_3(i\omega)\exp(i\omega T)}{(i\omega + \frac{b}{c})g'(\bar{v})}\right) \tag{3.18}$$

and

$$\delta_i(\omega, \bar{v}) := \Im\left(\frac{\tau p_3(i\omega)\exp(i\omega T)}{(i\omega + \frac{b}{c})g'(\bar{v})}\right). \tag{3.19}$$

Solving (3.17) with respect to $\bar{v}$ yields

$$\bar{v} = \phi_{1,2}(\omega) := \mp\sqrt{\frac{P+Q}{R}}, \tag{3.20}$$

with

$$\begin{aligned} P &:= \tan(\omega T)(c^2\tau\omega^4 + (c^3 - \tau(c^2 - b^2))\omega^2 - cb(1-b)), \\ Q &:= c^2(\tau c - 1)\omega^3 + (c^2 - b^2 - \tau cb(1-b))\omega, \\ R &:= c(\tan(\omega T) + \tau\omega)(c^2\omega^2 + b^2) \end{aligned}$$

provided that $\tan(\omega T) + \tau\omega \neq 0$ and $\sqrt{\frac{P+Q}{R}} \geq 0$. From (3.16) and (3.20) we obtain

$$q = \tilde{q}_{1,2} := -\omega\frac{c^2\tau^2\omega^4 - (\tau^2(c^2 - b^2) - c^2)\omega^2 - (c^2 - b^2)}{c^2\omega^2 + b^2)\gamma(\tau\omega\cos(\omega T) + \sin(\omega T))g'(\phi_{1,2}(\omega))}. \tag{3.21}$$

We are considering only the case of a unique existing stationary solution which implies that $q \leq \frac{c(1-b)}{bg'(0)}$. The loss of stability then takes places at the boundaries

$$\begin{aligned} \tilde{e}_1 &= \max_{\omega}\{\tilde{H}(\bar{v}_1(\omega)) - \frac{ac}{b} \quad : \quad q = \tilde{q}_1(\omega)\}, \\ \tilde{e}_2 &= \min_{\omega}\{\tilde{H}(\bar{v}_2(\omega)) - \frac{ac}{b} \quad : \quad q = \tilde{q}_2(\omega)\}. \end{aligned} \tag{3.22}$$

Provided that a and c are positive, $0 < b < 1$, $g \in C^2(\mathbb{R}, \mathbb{R})$ and $g''v < 0$ for all $v \neq 0$ the unique existing stationary solution of the neural system (3.1) is asymptotically stable if and only if $e \notin [\tilde{e}_1, \tilde{e}_2]$.
The curves $\tilde{e}_1(q)$ and $\tilde{e}_2(q)$ represent the potential Hopf bifurcation points of system (3.1). This dependence between $\tilde{e}$ and q is determined numerically and the result is shown in figure 3.1.

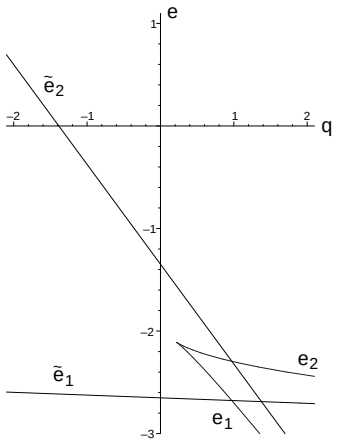

Figure 3.1: Stability chart of the stationary solution of the neural system (3.1). The curves $\tilde{e}_1$ and $\tilde{e}_2$ denote the transition points between stable stationary and unstable stationary behaviour. For $q > \frac{c(1-b)}{bg'(0)}$ there are two existing stationary solutions (curves e_1 and e_2). They can be read in equation (3.5). The simulation parameters are $(a, b, c, T, \tau) = (0.9,\ 0.9,\ 2.0,\ 30.0\ 40.0)$. Recalculated from [14].

3.3 Limiting case $T \to \infty$

In the case of $T \to \infty$ the loss of stability of the stationary solution is calculated. The results of this analysis can be directly related to the bifurcation structure of the iterated map. Let $(\bar{u}, \bar{v}, \bar{w}) \in \mathbb{R}^3$ be a stationary solution of the system (1.6). For the characteristic polynomial which was already calculated in the previous section holds

$$\chi(z) = p_3(z) - \frac{qg'(\bar{v})}{\tau}(z + \frac{b}{c}) \exp(-zT) = 0 \tag{3.23}$$

where p_3 is a third order polynomial

$$p_3(z) = (z + \frac{1}{\tau})(z^2 - c(1 - \frac{b}{c^2} - \bar{v}^2)z + b(\bar{v}^2 + \frac{1}{b} - 1)). \tag{3.24}$$

In order to obtain the limit of $T \to \infty$ we first scale the characteristic polynomial and replace z by $z = \frac{s}{T}$. For the corresponding expression for q we obtain in the limit case

$$q = \frac{c(\bar{v}^2 + \frac{1}{b} - 1) \exp(s)}{g'(\bar{v})}. \tag{3.25}$$

Since q is a real parameter, $s = i\omega$, $\omega \in I\!R$ is a solution of equation (3.25) if the imaginary part of q is equal to zero. Solving

$$\frac{c(\bar{v}^2 + \frac{1}{b} - 1) \sin(\omega)}{g'(\bar{v})} = 0 \tag{3.26}$$

yields the condition $\omega = k\pi$ with $k \in \mathbb{N}_0$. The stationary solution of the neural system loses its stability in the case of infinite delay if

$$q = \frac{c(\bar{v}^2 + \frac{1}{b} - 1)\cos(k\pi)}{g'(\bar{v})}, \qquad k \in \mathbb{N}_0. \tag{3.27}$$

The choice of k determines the type of bifurcation. In the special case of the basic parameters used in the calculations throughout this thesis ($(b, c) = (0.9,\ 2.0)$) and the sigmoidal function g having a positive derivative, odd k correspond to a Flip bifurcation whereas even k correspond to a saddle-node bifurcation. Restriction to the case $q = -1$ which was regarded for the iterated map leads to the choice of an even k and we obtain the following condition for the flip bifurcation points

$$g'(\bar{v}) = c(\bar{v} + \frac{1}{b} - 1). \tag{3.28}$$

Comparing this result with the linearisation of the iterated map at the fixed point for $q = -1$ (see equation (2.13))

$$g'(H^{-1}(U)) = H'(H^{-1}(U)) \tag{3.29}$$

and evaluating the auxiliary function

$$H(H^{-1}(U)) := c(\frac{1}{3}(H^{-1}(U))^3 + H^{-1}(U)(\frac{1}{b} - 1) - \frac{a}{b}) \tag{3.30}$$

leads to

$$g'(H^{-1}(U)) = c((H^{-1}(U))^2 + \frac{1}{b} - 1). \tag{3.31}$$

Equation (3.28) derived from the loss of stability of the stationary solution is equivalent to equation (3.31) that was obtained for the iterated map.
For the border case of $T \to \infty$ we obtain the following conclusion: The analysis has shown that the stationary solutions lose their stability at the flip bifurcation points of the iterated map.

3.4 Limiting case $\tau \to \infty$

The case of infinite time constant τ is related to an infinite refraction time of the postsynaptic potential. The characteristic polynomial of the linearisation (3.13) in this case becomes

$$\lim_{\tau \to \infty} \chi(z) = \chi_{\tau_\infty}(z) = z^3 - c(1 - \frac{b}{c^2} - \bar{v}^2)z^2 + b(\bar{v^2} + \frac{1}{b} - 1)z. \tag{3.32}$$

The case $\tau \to \infty$ leads to a decoupling of the network equation and the FitzHugh-Nagumo subsystem. u becomes constant and can therefore no longer determine

the stability of the system. The dynamics of the system is then determined by the remaining FitzHugh-Nagumo system with u regarded as bifurcation parameter.

$$\begin{aligned} \dot{v}(t) &= c(w(t) + v(t) - \frac{1}{3}v^3(t)) + u, \\ \dot{w}(t) &= (a - v(t) - bw(t))/c. \end{aligned} \tag{3.33}$$

The bifurcation behaviour of the FitzHugh-Nagumo system is well studied by several authors [12, 17, 24, 35]. We therefore give only a short summary of the main bifurcational results that are specified in [14]. The results concerning the FitzHugh-Nagumo system are used in the discussion of bifurcation results obtained in the further course of the thesis.

Lemma 3.2 *(Hopf bifurcation)*
Assume $a, c > 0$, $0 < b < 1$ and $b > c^2$. With

$$u^{(l)} = \frac{c}{\gamma}[\frac{1}{3}{v^{(l)}}^3 + (\frac{1}{b} - 1)v^{(l)} - \frac{a}{b}], \tag{3.34}$$

where

$$v^{(l)} = (-1)^l\sqrt{1 - \frac{b}{c^2}}\,; \quad l = 1, 2\,, \tag{3.35}$$

there holds:
If $\frac{1}{2} < b < 1$ and $c^2 > \frac{b^2}{2b-1}$, equation (1.3) undergoes a subcritical Hopf bifurcation at $u = u^{(l)}$, $l = 1, 2$. This means, there are positive numbers ε_1, ε_2 such that (1.3) has a periodic solution for $u \in (u^{(1)} - \varepsilon_1, u^1)$ and $u \in (u^{(2)}, u^{(2)} + \varepsilon_2)$. The bifurcating periodic solutions are unstable.

Lemma 3.3 *(Global existence and nonexistence of periodic solutions)*
Assume $a, c > 0$, $0 < b < 1$ and $b > c^2$. There are real numbers $u^{(1')}$, $u^{(2')}$ with $u^{(1')} \le u^{(1)} < u^{(2)} \le u^{(2')}$, $u^{(1)}$ and $u^{(2)}$ as in Lemma 3.2, such that:
For $u < u^{(1')}$ and $u > u^{(2')}$ equation (1.3) has no nonconstant periodic solutions. In this case the unique existing stationary solution of (1.3) is globally asymptotically stable.
For $u^{(1')} < u < u^{(2')}$ equation (1.3) has a nonconstant periodic solution.

Lemma 3.4 *(Uniqueness and Stability of periodic solutions)*
Assume $a, c > 0$, $\frac{1}{2} < b < 1$ and $b > c^2 > \frac{b^2}{2b-1}$.
For $u^{(1)} < u < u^{(2)}$, $u^{(1)}$ and $u^{(2)}$ as in Lemma 3.2, equation (1.3) has a unique periodic solution, which is asymptotically orbitally stable.

Remark 3.1 (Bistability and saddle-node bifurcation of periodic solutions)
Assume $\frac{1}{2} < b < 1$ and $b > c^2 > \frac{b^2}{2b-1}$.
A numerical calculation (see Figure 3.2) performed using [7] indicates that for $u^{(1')} < u < u^{(1)}$ and $u^{(2)} < u < u^{(2')}$ there are exactly two periodic solutions,

a stable and an unstable one. In this case (1.3) is bistable. Notice that the interior and the exterior of the trajectory of the unstable periodic solution are the attraction domains of the stable stationary and the periodic solution, respectively. At $u = u^{(1')}$ and $u = u^{(2')}$ saddle-node bifurcations of periodic solutions occur.

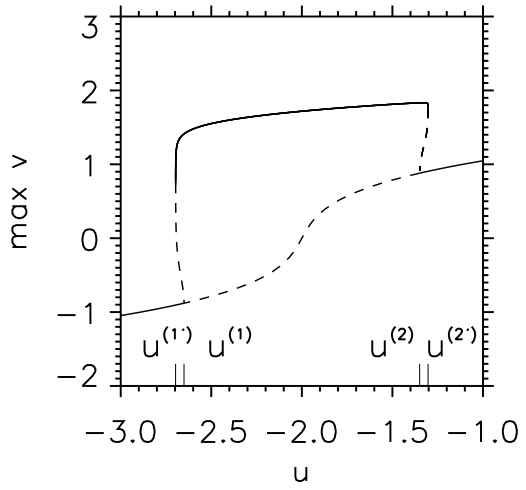

Figure 3.2: Bifurcation diagram of the FitzHugh-Nagumo subsystem with parameter u.

Numerical calculations using the parameters ($a = b = 0.9$ and $c = 2.0$) yield that the FitzHugh-Nagumo oscillator (1.3) has a subcritical Hopf bifurcation for $u = u^{(1)} = -2.6505$ and $u = u^{(2)} = -1.3495$. From Lemma (3.3) and Remark (3.1) the oscillation interval I_{osc} of (1.3) can be calculated:

$$I_{osc} = [u^{(1')}, u^{(2')}] = [-2.6969, -1.3031].$$

Chapter 4

Numerical bifurcation analysis

In contrast to the two previous chapters where the bifurcation behaviour of the neural model was analysed for the limiting case of infinite delay with the help of analytical methods this chapter contains a numerical bifurcation analysis of the neuron model for different time delays.
Numerical bifurcation results for our model were until now only achieved for the underlying FitzHugh-Nagumo subsystem that consists of ordinary differential equations, see for example [14]. A numerical bifurcation analysis for the whole model that contains a time delay was still to be found. In contrast to ordinary differential equations retarded differential equations require special numerical bifurcation techniques. In the case of ordinary differential equations a lot of numerical software exists to analyse the bifurcation behaviour. To our knowledge for delayed differential equations there exists only one software that is able to deal with bifurcations of delay differential systems. This software is called DDE-BIFTOOL (a matlab package for numerical bifurcation analysis of delay differential equations with several fixed, discrete delays), version 2.00 [9] and was developed by Koen Engelborghs and coauthors at the University of Leuven, Belgium. DDE-BIFTOOL was applied successfully on bifurcation problems for systems with time delay. For example mathematical models for semiconductor lasers with delayed feedback due to reflections on optical fibers were analysed with DDE-BIFTOOL [22, 15] as well as mathematical models for blood cell production [2].
To prepare the numerical bifurcation analysis of our delayed neuron model we first give a short introduction of the underlying theoretical methods for the bifurcation analysis of delayed differential systems. On the basis of the introductory remarks we first determine the stationary solutions of the neural system and analyse the characteristic roots of the steady state with regard to the parameter e. With that is is possible to detect the specific points of bifurcation. Starting from the bifurcation point the branch of periodic solutions is calculated and so the bifurcation diagram with respect to the bifurcation parameter e is drawn up. The stability along the branch of periodic solutions is determined using the Floquet

multipliers. Stable as well as instable sections are found.
A calculation of the bifurcation diagram for large time delays completes the numerical bifurcation analysis and facilitates a comparison with the results of the previous chapters that were obtained for infinite delay.
A comparison of the results of the different approaches to bifurcation analysis of the neural system from chapter 2 (iterated map), chapter 3 (bifurcation properties of the neural system) and chapter 4 (numerical bifurcation analysis) is carried out in the following chapter 5.

4.1 Bifurcation analysis of delay differential equations

The purpose of this section is to provide a short summary of the bifurcation analysis of delayed differential systems. In part, we follow [27, 26]. A detailed description of delayed differential systems and bifurcation analysis can be found in [6, 19, 28, 8].

4.1.1 Theoretical approach

In order to adapt it to our neuron model we restrict the further description of retarded differential equations to systems with one constant delay. The general form of a retarded differential system is then

$$\begin{aligned} \dot{x}(t) &= f(x(t), x(t-T), \eta) && \text{for } t > 0, \\ x(t) &= \varphi && \text{for } -T \leq t \leq 0. \end{aligned} \tag{4.1}$$

The spaces for the variables and parameters are: $x \in \mathbb{R}^n$, the delay $T \in \mathbb{R}$ and the parameters $\eta \in \mathbb{R}^p$. For the function f which represents the right-hand derivative holds

$$f : \mathbb{R}^{2n} \times \mathbb{R}^p \to \mathbb{R}^n. \tag{4.2}$$

In contrast to ordinary differential equations it is necessary to know the entire history of $x(0)$ to obtain a unique solution. The history is a continous function on the interval $[-T, 0]$. This denotes that the phase space of (4.1) is an infinite dimensional space of continous functions denoted by C which maps into the space $\mathbb{R}^n$

$$\varphi : [-T, 0] \to \mathbb{R}^n \tag{4.3}$$

with the history $\{\varphi(t) \mid t \in [-T, 0)\}$ and the head $\varphi(0)$. The temporal evolution of every point φ in the phase space C is determined by equation (4.1) for any positive t and can be described by an evolution operator

$$\Phi^t : C \to C. \tag{4.4}$$

The solution of (4.1) starting from a point φ in C is then given by

$$x : [0, \infty) \to I\!R^n, \qquad t \to \Phi^t(\varphi). \tag{4.5}$$

Steady states of (4.1) are points φ_0 such that $\varphi_0(t) = x_0 \ \forall \ t \in [-T, 0]$ and fixed $x_0 \in I\!R^n$. This is equivalent to $f(x_0, x_0, \eta_0) = 0$ for fixed parameter values η_0. The stability of the fixed point is given by the eigenvalues of the linearisation

$$Df(x_0, x_0, \eta_0) = Df(x_0, x_0, \eta_0)\, x(t) + Df(x_0, x_0, \eta_0)\, x(t - T) \tag{4.6}$$

around the fixed point. For x(t) we use the ansatz

$$x(t) = \exp(zt)\ \xi \tag{4.7}$$

and joining this together leads to the characteristic equation of the system

$$\chi(z) = \det(zI - A(x_0, x_0, \eta_0) - B(x_0, x_0, \eta_0)\, e^{-z\,T}) = 0. \tag{4.8}$$

In contrast to ordinary differential equations the characteristic equation is transcendental and posseses an infinite number of eigenvalues. In the case of fixed delays the eigenvalues are discrete and the eigenvalues have an important property that is given in the next theorem.

Theorem 4.1 *Given any real number ρ, equation (4.8) has no more than a finite number of roots z such that $Re\, z \geq \rho$.*

Further informations on this theorem can be found in [8, 19].
In analogy to the definition of hyperbolicity for maps in definition 2.1 hyperbolic steady states of retarded differential equations can be defined. They have no eigenvalues of the characteristic equation that have zero real part.
Nonhyperbolic steady states of retarded differential equations show two types of local bifurcations of codimension one:

- Saddle-node bifurcation: a single real eigenvalue goes through zero.
- Hopf bifurcation: a complex conjugate pair of eigenvalues crosses the imaginary axis.

A solution $x(t)$ of (4.1) is called periodic if it is starting from a point $q \in C$ with the property $\Phi^P(q) = q$ for the period P. The periodic orbit Γ contains all q with $\Phi^P(q) = q$. In order to determine the stability of the periodic orbit we first introduce the notion Poincaré map Π.

Definition 4.1 *Let Γ be a periodic orbit of the flow Φ^t and $\Sigma \subset I\!R^n$ be a hyperplane perpendicular to Γ. If $\Sigma \subset I\!R^n$ is fixed and C_Σ denotes the space of points in C whose heads are lying in Σ then the Poincaré map $\Pi : C_\Sigma \to C_\Sigma$ is defined as*

$$\Pi(\varphi) = \Phi^{t_q}\, \varphi \tag{4.9}$$

with $t_q > 0$ being the return time to Σ.

The stability of the periodic orbit can be calculated with the help of the Floquet multipliers. They are the eigenvalues of the linearisation $D\Pi(q)$ of the Poincaré map around the fixed point $q \in C_\Sigma$.
Hyperbolicity in terms of periodic orbits means that there is no Floquet multiplier lying on the unit circle except the trivial Floquet multiplier at +1. Periodic orbits of codimension one can display three basic local bifurcations if the hyperbolicity condition is violated:

- Saddle-node bifurcation: a single real eigenvalue goes through +1.
- Period doubling bifurcation: a single real eigenvalue goes through -1.
- Neimark-Sacker (or torus) bifurcation: a complex conjugate pair of Floquet multipliers moves through the unit circle of the complex plane at $e^{2\pi i\alpha}$ with $\alpha \neq 0, \frac{1}{2}, \frac{1}{3}, \frac{2}{3}, \frac{1}{4}, \frac{3}{4}$.

4.2 Numerical analysis of the bifurcations

This section contains the numerical bifurcation analysis of the neural system using DDE-BIFTOOL. After a short description of this tool, we calculate the bifurcation diagram of the neural system for the delay $T = 30$ and for large delay $T = 1000$ in order to compare the results with the calculations of the previous chapters for infinite delay.

4.2.1 DDE-BIFTOOL

The numerical bifurcation analysis of our neuron model was carried out with DDE-BIFTOOL, version 2.00 [9]. DDE-BIFTOOL is a collection of MATLAB routines for the numerical analysis of delay differential equations. The package contains various routines to analyse steady state solutions and periodic solutions of delay differential equations. After a steady state has been found it can compute the eigenvalues of the characteristic equation and it allows to determine the rightmost root that is decisive for the stability of the system. A correction of the eigenvalues follows using Newton iterations. DDE-BIFTOOL is able to compute and to continue Hopf bifurcations and saddle-node bifurcations from steady states. Furthermore, it can detect the local codimension one bifurcations of periodic orbits (saddle-node bifurcations, period doubling bifurcations and Neimark-Sacker bifurcations) using orthogonal collocation. In addition adaptive mesh selection can be chosen to improve the results. In order to determine the stability of points on the branch of periodic solutions the package provides also routines to calculate the largest Floquet multipliers.

4.2.2 Steady state solutions

Starting from our basic neuron model

$$\begin{aligned} \tau\dot{u}(t) &= -u(t) + qg(v(t-T)) + e, \\ \dot{v}(t) &= c(w(t) + v(t) - \frac{1}{3}v^3(t)) + u(t), \\ \dot{w}(t) &= (a - v(t) - bw(t))/c \end{aligned} \tag{4.10}$$

we first determine the stationary solutions which have been already defined in equation (3.2)

$$\begin{aligned} \tilde{H}(v) &:= \tfrac{c}{3}v^3 + c(\tfrac{1}{b} - 1)v - qg(v) = e + \tfrac{ac}{b}, \\ u &= qg(v) + e, \\ w &= \tfrac{a-v}{b}. \end{aligned} \tag{4.11}$$

We consider only the case of a unique existing solution (see lemma 3.1) which holds for

$$c(\frac{1}{b} - 1) \geq qg'(0) \tag{4.12}$$

as condition on the parameters. The most important bifurcation parameter is the external signal e for which a numerical bifurcation analysis is given in this chapter. Numerical calculations have shown that the variation of the external signal e causes a destabilisation of the system that leads to periodic oscillations in the form of bursting and spiking. Consecutively a fixed set of basic parameters was used in the bifurcation analysis $(a, b, c, q, \tau, T) = (0.9, 0.9, 2.0, -1.0, 40, 30)$. The steady state solution was computed numerically and we obtain for the given set of parameters and a starting value of $e = -2.5$ the points ($u^* = -2.5374,\ v^* = -0.8120,\ w^* = 1.9022$). Solving the characteristic equation

$$\chi(z) = \det(z\mathbf{1} - A - Be^{-zT}) = 0 \tag{4.13}$$

with A and B given in (3.10) we obtain the rightmost roots which are shown in figure (4.1). The left picture shows the rightmost correctly computed characteristic roots of the steady state that were calculated up to $\Re(z) \geq -0.04$. The red colour denotes unstable roots and the green color corresponds to stable roots. In the right picture the characteristic roots were calculated up to $\Re(z) \geq -0.3$. The calculation was extended in direction to lower real part in order to obtain more roots. There it is possible to see a small discrepancy between approximated and corrected roots. The calculations of the characteristic roots show that the steady state solution is unstable because a pair of characteristic roots with positive real part $\Re(z) \approx 0.118$ was found.

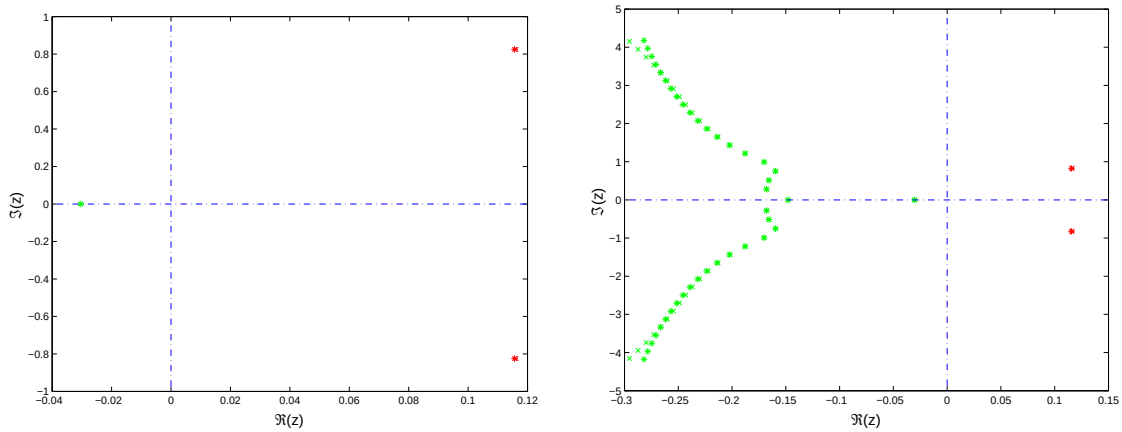

Figure 4.1: Approximated ($\times$) and corrected ($*$) roots of (1) at u^*, v^*, w^*. Left: Correctly computed roots up to $\Re(z) \geq -0.04$. Right: Roots calculated up to $\Re(z) \geq -0.3$.

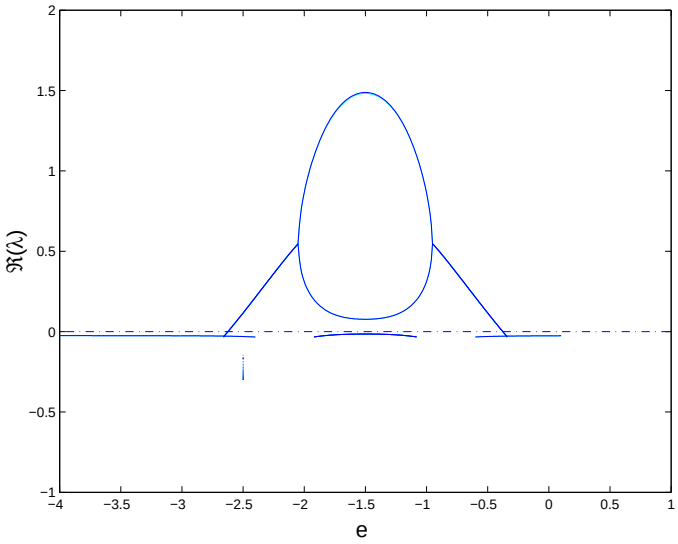

Figure 4.2: Real part of the characteristic roots of (1) at u^*, v^*, w^*.

4.2.3 Periodic solutions

The real part of the roots of the characteristic equation (4.13) can now be evaluated with respect to the bifurcation parameter e, see figure 4.2. It can be seen that there are two points at which the real part of the characteristic roots is zero. This could correspond to a Hopf bifurcation of steady states. The two possible Hopf points e_1^*, e_2^* can be determined numerically. The next step is to clarify whether the two Hopf point candidates fulfill the Hopf criterium of a complex conjugate pair of eigenvalues that cross the imaginary axis. Figure 4.3 shows that there is indeed a complex conjugate pair passing the imaginary axis and this confirms that we have found two Hopf bifurcation points e_1^* and e_2^*.
Starting from the Hopf bifurcation point e_1^* the branch of periodic solutions is followed in a two parameter space. Subsequently the branches of periodic solutions can be calculated in dependence on the bifurcation parameter e. Figure 4.4 shows

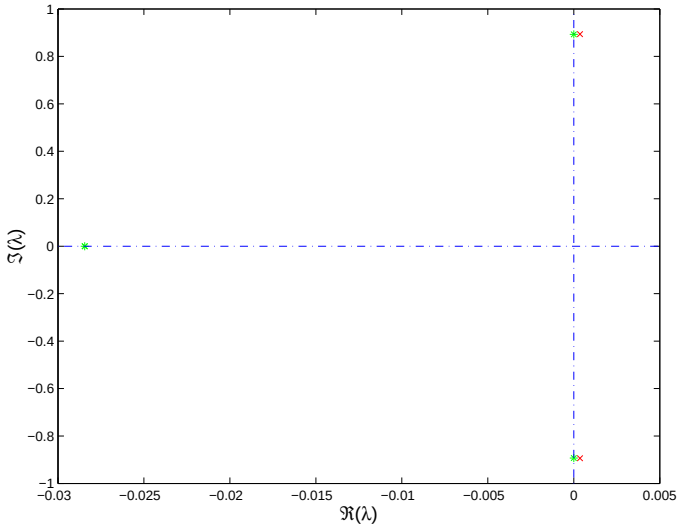

Figure 4.3: Characteristic roots at Hopf point e_1^*.

the computation of the branch of periodic solutions with regard to the bifurcation parameter e. Predictions of the branch were plotted in green, corrections are plotted in blue. It is visible that the numerical calculation was difficult in some regions of the bifurcation diagram due to the discrepancy between predictions and corrections. The dots indicate the underlying mesh.
To determine the bifurcation direction of the periodic solution the branch was followed for a small number of points in the vicinity of the Hopf bifurcation point. Figure 4.5 displays the branch of periodic solutions which is drawn in blue. The branch of steady states is plotted in red. This reveals that the transition from stationary to periodic solutions occurs via a subcritical Hopf bifurcation.
The whole bifurcation diagram displaying the branch of periodic v solutions in dependence on the bifurcation parameter e is drawn in figure 4.6. The red line

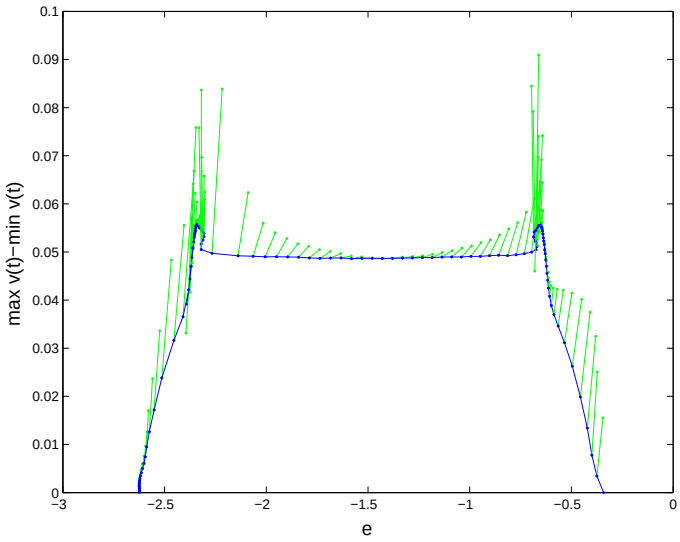

Figure 4.4: Predictions and corrections of the periodic solution branch. The branch emanates from the Hopf point e_1^* and displays the predictions (green color) and corrections (blue color) along the branch. The mesh is represented by the dots.

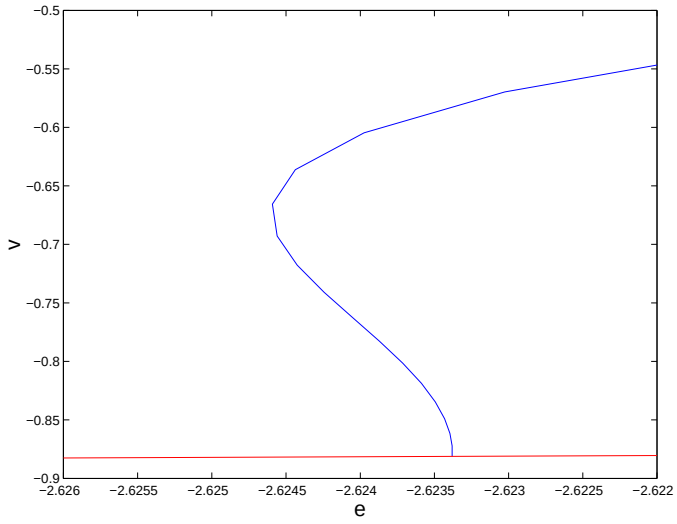

Figure 4.5: Part of the bifurcation diagram for the membrane potential v in the vicinity of the bifurcation with respect to the parameter e. This figure demonstrates the subcritical Hopf bifurcation. The red line shows the stationary solution and the blue line represents the envelope of the maxima of the periodic v solutions.

displays the steady state solution and the blue lines indicate the branches of periodic v solutions that emanate from the two Hopf points e_1^* and e_2^*. The period

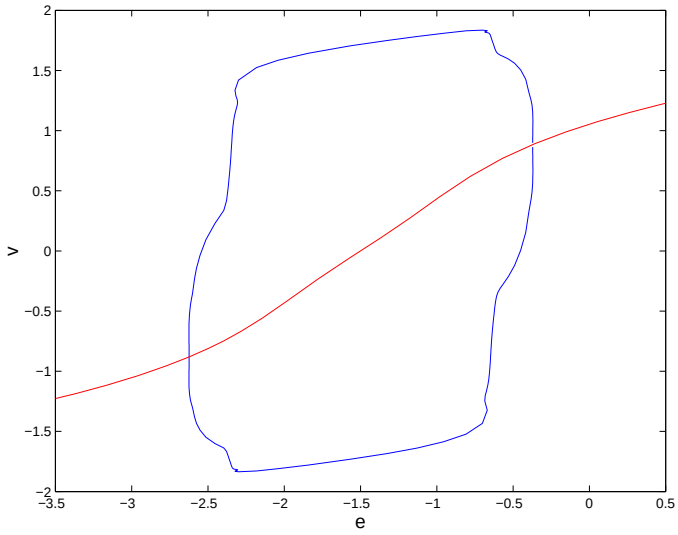

Figure 4.6: Bifurcation diagram for the branch of periodic v solutions with respect to the bifurcation parameter e. The red line represents the stationary solution v^* and the blue lines depict the envelope of the periodic v solutions.

of the periodic orbits as a function of the bifurcation parameter e is shown in figure 4.7.
The stability of the periodic solution can be determined by calculating the Floquet multipliers for each point located on the branch of the periodic solutions. For three selected points on the branch of periodic solutions the Floquet multipliers are calculated in order to obtain information about the stability structure of the branch. The approximate position of the chosen points is drawn in figure 4.8 and the Floquet multipliers themselves are displayed in figures 4.9, 4.10 and 4.11.
As we can see from the different configurations of the three Floquet multipliers the branch of periodic solutions for parameter values of e lying in the interval of $e \in [e_1^* = -2.62; -2.32]$ shows a complex structure of a mixture of stable and unstable points. The Floquet multipliers indicate unstable behaviour that corresponds to saddle-node bifurcations as well as period doubling bifurcations and Neimark-Sacker bifurcations for this part of the branch. It seems to be that these stability changes do not correspond to real bifurcation points of the branch of periodic solutions but seem to be caused by computational difficulties. We have already seen that right in the interval $e \in [e_1^* = -2.62; -2.32]$ there exist big discrepancies between predictions and corrections of the periodic solutions which was shown in figure 4.4.
To summarise we can say that it is not clear what happens definitely with

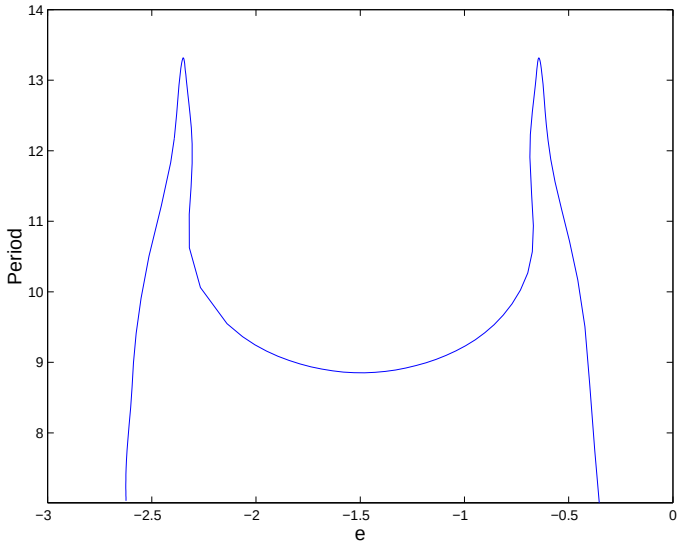

Figure 4.7: Period of oscillation of the periodic orbits with respect to the bifurcation parameter e.

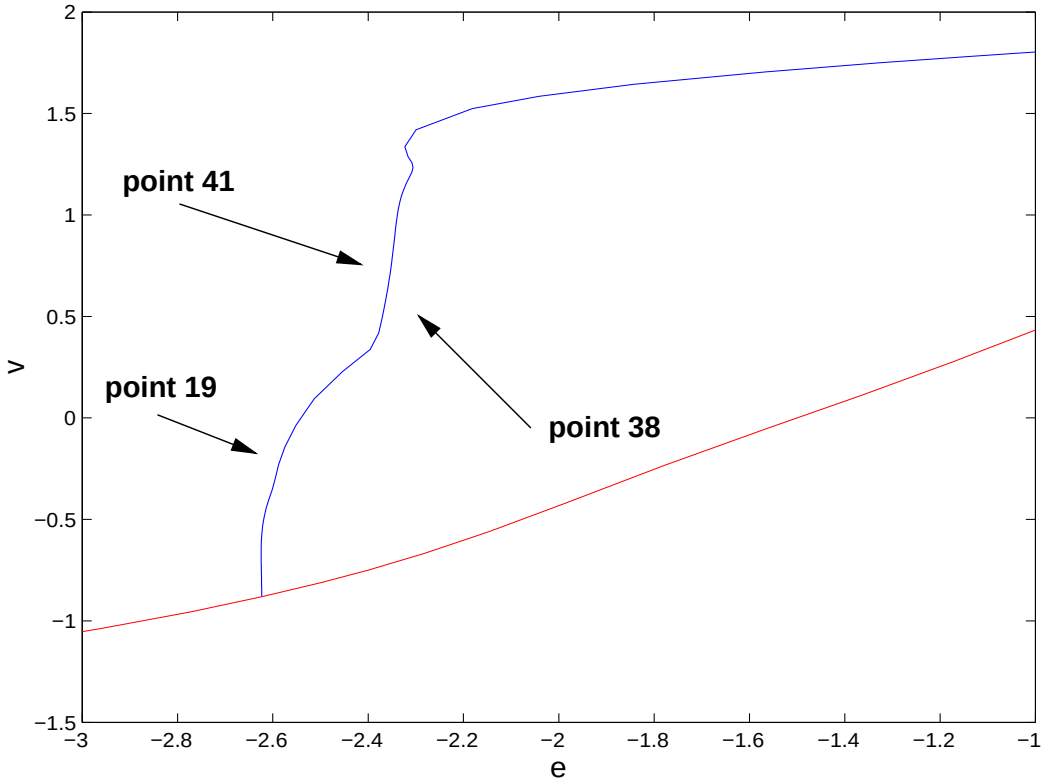

Figure 4.8: Branch of periodic solutions.

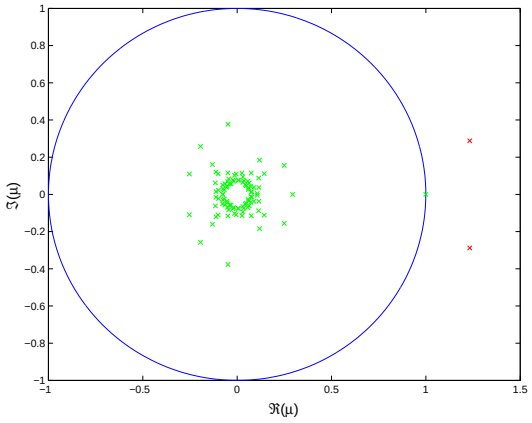

Figure 4.9: Floquet multipliers of point 19 on the branch of periodic solutions.

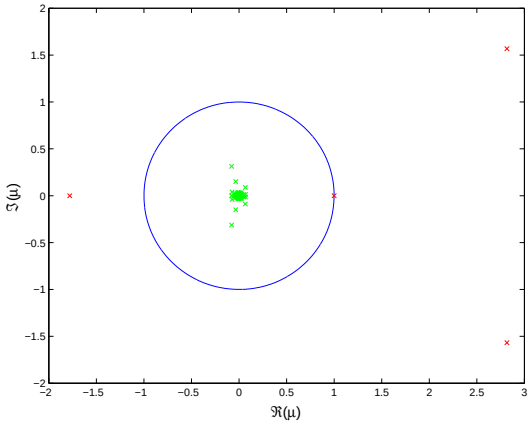

Figure 4.10: Floquet multipliers of point 38 on the branch of periodic solutions.

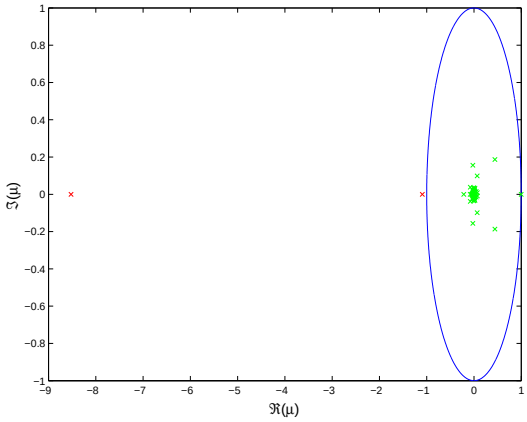

Figure 4.11: Floquet multipliers of point 41 on the branch of periodic solutions.

the branch of periodic solutions in the region that corresponds to $e \in [e_1^* = -2.62; -2.32]$. It seems to be a rather unstable part of the branch of periodic solutions.
However, in the middle of the branch there is a range of periodic solutions that have Floquet multipliers which are all located inside the unit circle and which correspond to stable behaviour. This stable part of the branch starts at the related parameter value $e = -2.32$ and ends at $e \approx -0.71$.
The information obtained by the numerical bifurcation analysis of the neural system is now compared with the periodic solutions of the neural system (4.10) which were computed using the software XPPAUT [10], with which it is possible to calculate the solutions of delay differential equations.

The region of instability on the branch of periodic solutions corresponds to the bursting regime of the neural system (see figure 4.12, left picture). The simulation shows solutions for $e = -2.5$ displaying bursting. Spiking can be found for the stable part of the branch. The numerical simulation in figure 4.12, right picture, displays this spiking for $e = -2.0$.
With this a possible explanation for the numerical difficulties in continuing the branch of periodic solutions can now be found. Since numerical simulations indicate that bursting occurs for parameter values of e that correspond to the unstable part of the branch the numerical calculation in this region has to treat a system that displays a permanent change from oscillatory dynamics to quasistationary behaviour. During bursting the interaction of the two time scales of the model is especially visible. This may cause problems in following the branch of periodic solutions and computing the Floquet multipliers in the bursting region.
The spiking region always shows stable behaviour and there seems to be no numerical difficulty. This can be attributed to the permanent oscillations during spiking which do not turn into quasistationary behaviour.

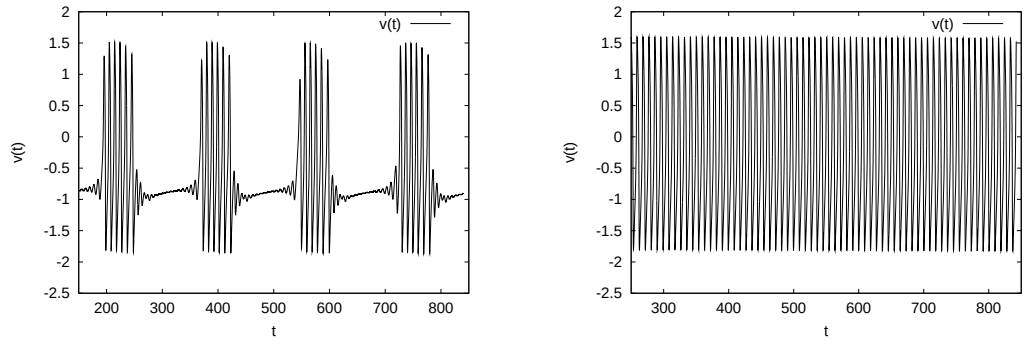

Figure 4.12: Numerical simulations of the membrane potential $v(t)$ with parameters $(a, b, c, q, \tau, T) = (0.9, 0.9, 2.0, -1.0, 40, 30)$ with XPPAUT. Left: Periodic solution for $e = -2.5$ displaying bursting. Right: Periodic solution for $e = -2.0$ displaying spiking.

To conclude this section the point where the stable part of the branch of periodic solutions begins is compared with numerical solutions of the neural system. The analysis with DDE-BIFTOOL revealed that the branch of periodic solutions becomes stable for $e > e_{stable} = -2.32$. Looking at the periodic solution of the neural system around e_{stable} in figure 4.13 calculated with XPPAUT shows that the transition between bursting and spiking takes place right there. The transition occurs for $e = -2.34$ which is close to the value calculated with DDE-BIFTOOL.

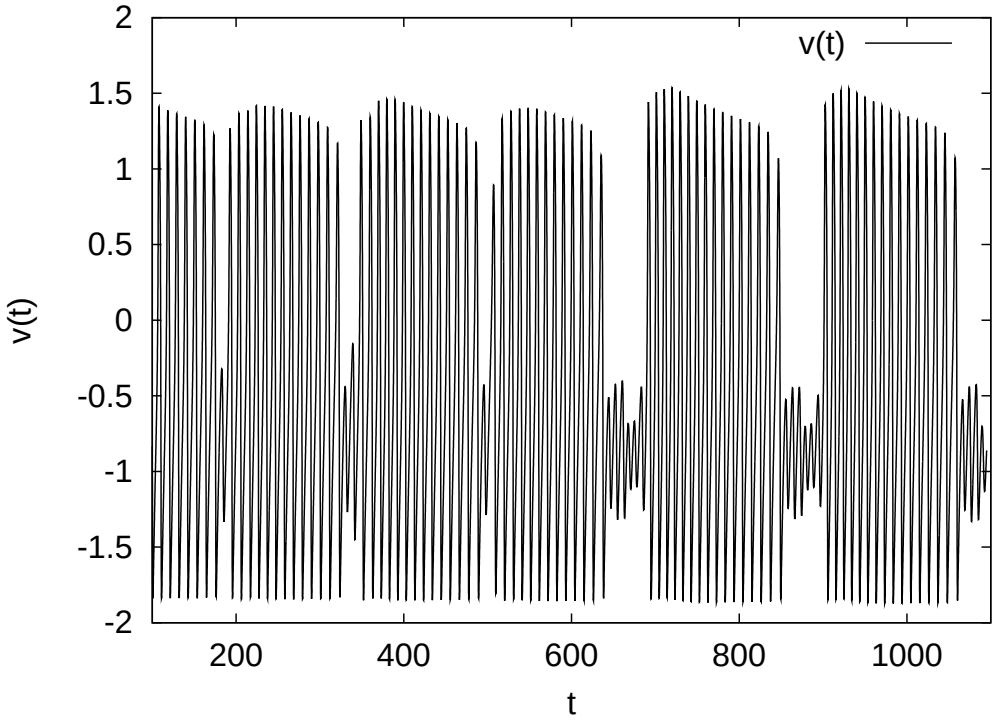

Figure 4.13: The transition from bursting to spiking takes place at a value of $e = -2.34$ for the bifurcation parameter (calculated with XPPAUT). This corresponds very well to the transition point $e_{stable} = -2.32$ that was calculated with DDE-BIFTOOL.

4.3 Numerical bifurcation analysis for large time delay

This last section of the numerical bifurcation analysis of the neural model shows the results of the bifurcation analysis for a large time delay $T = 1000$. Similar to the proceeding in the previous section we first calculate the steady state solution and determine the bifurcation points with respect to the parameter e. Starting

from the Hopf points the branches of periodic solutions are followed and the bifurcation diagram is calculated. Figure 4.14 shows the branches of periodic v solutions with regard to the bifurcation parameter e for $T = 1000$. The branch of steady states is drawn in red and the branches of periodic solutions are plotted in blue.
For calculations with DDE-BIFTOOL for large delay T ($T = 10000$) it turned out that DDE-BIFTOOL is not able to calculate a complete bifurcation diagram. For that reason also the calculated bifurcation diagram for $T = 1000$ has to be regarded sceptically especially with respect to the direction of bifurcation and the shape of the branches. Calculations of the solution of the neuron model carried out with XPPAUT confirm this lack of abilities of DDE-BIFTOOL.
However, the comparison with results of the iterated map show that for $T = 1000$ the bifurcation points calculated with DDE-BIFTOOL are plausible.

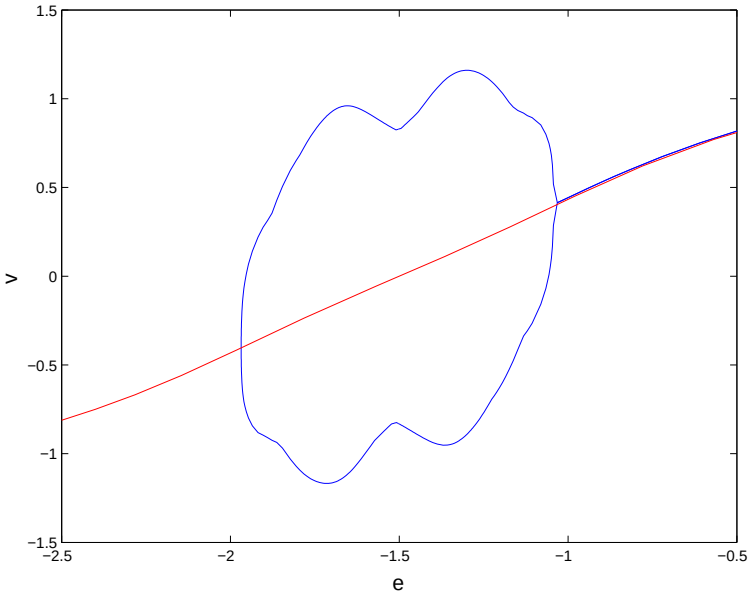

Figure 4.14: Branches of periodic solutions for large time delay $T = 1000$ with regard to the bifurcation parameter e. The red line depicts the branch of steady state solutions and the branches of periodic solutions are depicted by blue lines.

In contrast to the bifurcation diagram 4.6 for time delay $T = 30$ the region of periodic solutions has shrunk and the amplitude of the branch of periodic solutions became smaller. In addition the shape of the branch of periodic solutions changed.

Chapter 5

Comparison of analytical and numerical results

It is the purpose of this chapter to compare and to combine the results of the three previous chapters in order to find an explanation of the bursting behaviour of our neuron model

$$\begin{aligned} \tau\dot{u}(t) &= -u(t) + qg(v(t-T)) + e, \\ \dot{v}(t) &= c(w(t) + v(t) - \frac{1}{3}v^3(t)) + u(t), \\ \dot{w}(t) &= (a - v(t) - bw(t))/c. \end{aligned} \tag{5.1}$$

Chapter 2 contains the concept of the iterated map. The neural system has been investigated there for the limit case of infinite delay. The iterated map facilitates an analytical bifurcation analysis (with support of some numerical calculations) in the case of infinite delay. As a result the range of periodic solutions was determined as well as the direction of bifurcation.
A different approach of analysing the bifurcation behaviour of (5.1) is given in chapter 3. Starting from the stationary solution we calculated mainly analytically the potential Hopf points where the stationary solutions become unstable. The loss of stability of the stationary solutions was also calculated for infinite delay T which led to the same bifurcation points as for the iterated map.
The third approach to obtain information about the bifurcation behaviour of the neuron model was a numerical bifurcation analysis that was carried out in chapter 4. Bifurcation diagrams and bifurcation directions were determined for two different delays.
A detailed comparison of the three approaches is carried out in the following subsections and a conclusion for the occurence of bursting is drawn from the results.

5.1 Results for finite delay

An analytical result for finite delay is the stability diagram of the stationary solution for the parameter set $(a, b, c, T, \tau) = (0.9,\ 0.9,\ 2.0,\ 30.0,\ 40.0)$ calculated from the loss of stability of the stationary solutions. The two curves $\tilde{e}_1$ and $\tilde{e}_2$, see figure 5.1, represent the potential Hopf points of the neural system in dependence on the coupling parameter q. The case of $q = -1$ is depicted by the green line and yields two potential Hopf bifurcation points. These are related

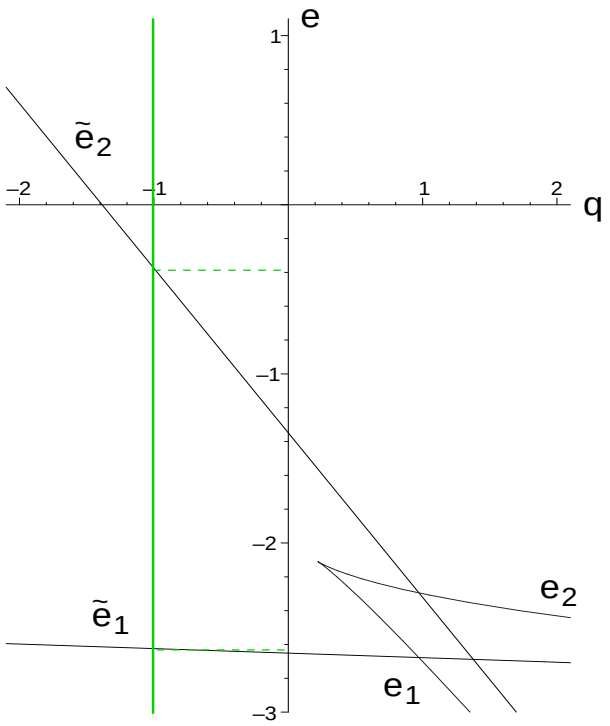

Figure 5.1: Hopf points calculated from the loss of stability of the stationary solutions. The solid green line emphasizes the case $q = -1$ and the dashed green lines refer to the corresponding value of e.

to parameter values $e_1^{Hopf} \approx -2.62$ and $e_2^{Hopf} \approx -0.39$ (dashed green lines). This is in perfect agreement with the numerical bifurcation analysis that was carried out with DDE-BIFTOOL. For the parameter values $(a, b, c, q, T, \tau) = (0.9,\ 0.9,\ 2.0,\ -1.0,\ 30.0,\ 40.0)$ the DDE-BIFTOOL bifurcation diagram is shown in figure 5.2. So the numerical bifurcation analysis with DDE-BIFTOOL confirms that the potential Hopf points are indeed Hopf bifurcation points.

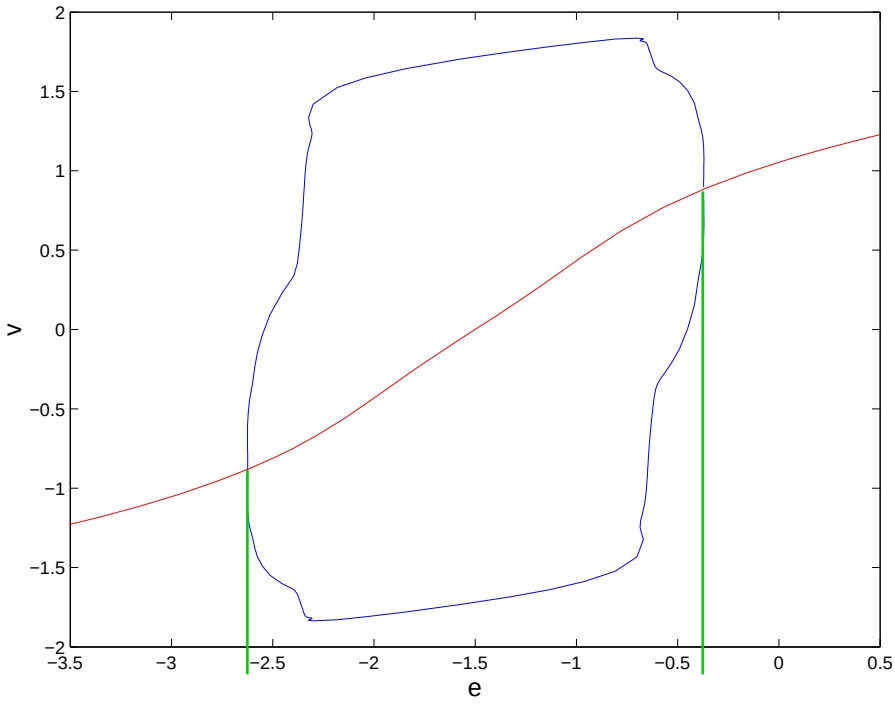

Figure 5.2: Hopf points calculated with the numerical bifurcation analysis using DDE-BIFTOOL. The solid green lines mark the two Hopf bifurcation points and refer to the corresponding e values.

5.2 Results for infinite and large delay

The bifurcation points for infinite delay have been calculated with the iterated map and with the loss of stability of the stationary solutions. Both methods deliver the same bifurcation points.
For our standard set of parameters $(a, b, c, q, T, \tau) = (0.9,\ 0.9,\ 2.0,\ -1.0,\ 30.0,\ 40.0)$ the iterated map on the one hand has two bifurcation points at

$$e_1^{flip} = -1.97 \qquad e_2^{flip} = -1.03 \tag{5.2}$$

that were calculated using an analytical approach. The corresponding bifurcation diagram of the iterated V-map is drawn in figure 5.3.

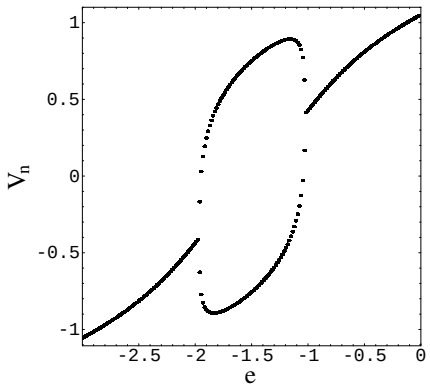

Figure 5.3: Bifurcation diagram of the iterated V-map for infinite delay.

The numerically calculated bifurcation diagram for the v branch of periodic solutions (figure 5.4) using DDE-BIFTOOL on the other hand shows the behaviour of the system for a large time delay $T = 1000$. The bifurcation points are the same than those calculated using the iterated map for infinite delay.

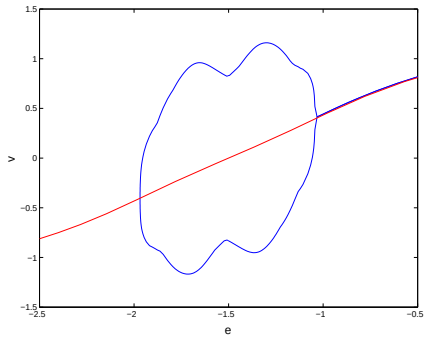

Figure 5.4: Bifurcation diagram of the branch of periodic v solutions for delay $T = 1000$.

5.3 Bursting in relation to the iterated map

To complete the analysis of the iterated map we examined the connection between the FitzHugh-Nagumo subsystem and the bifurcation structure of the iterated map. The FitzHugh-Nagumo subsystem has already been described in section 3.4 and we know that its periodic solutions emanate from the stationary solution via a subcritical Hopf bifurcation. The interval of oscillations I_{osc} in dependence on the parameter u has been calculated in [14] and it holds

$$I_{osc} = [u^{(1')}, u^{(2')}] = [-2.6969, -1.3031].$$

Drawing together the iterated U-map and the oscillation interval I_{osc} of the FitzHugh-Nagumo system shows that the region of periodic solutions of the iterated U-map lies completely within the oscillation interval, see figure 5.5.

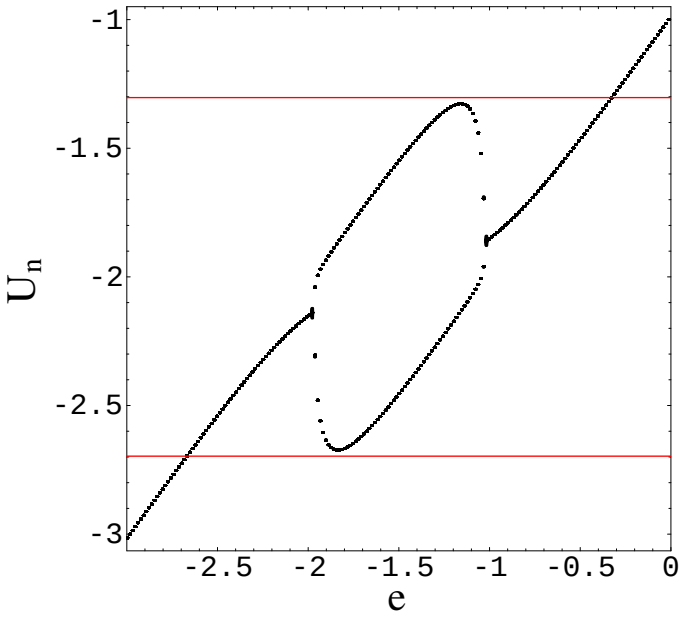

Figure 5.5: The iterated U-map plotted together with the borders of the oscillation interval of the FitzHugh-Nagumo subsystem (drawn in red).

In order to clarify the connection between the iterated map, the oscillation interval of the FitzHugh-Nagumo oscillator and the behaviour of the neural system (5.1) we calculated its solutions for a large time delay $T = 10000$ and for various values of parameters $e \in [-2.7, -0.2]$ with XPPAUT. The result sketched in figure 5.6 is very instructive.
On the basis of the calculation of the iterated map and numerical calculations of the neuron model for large delays we can draw the following conclusions on the

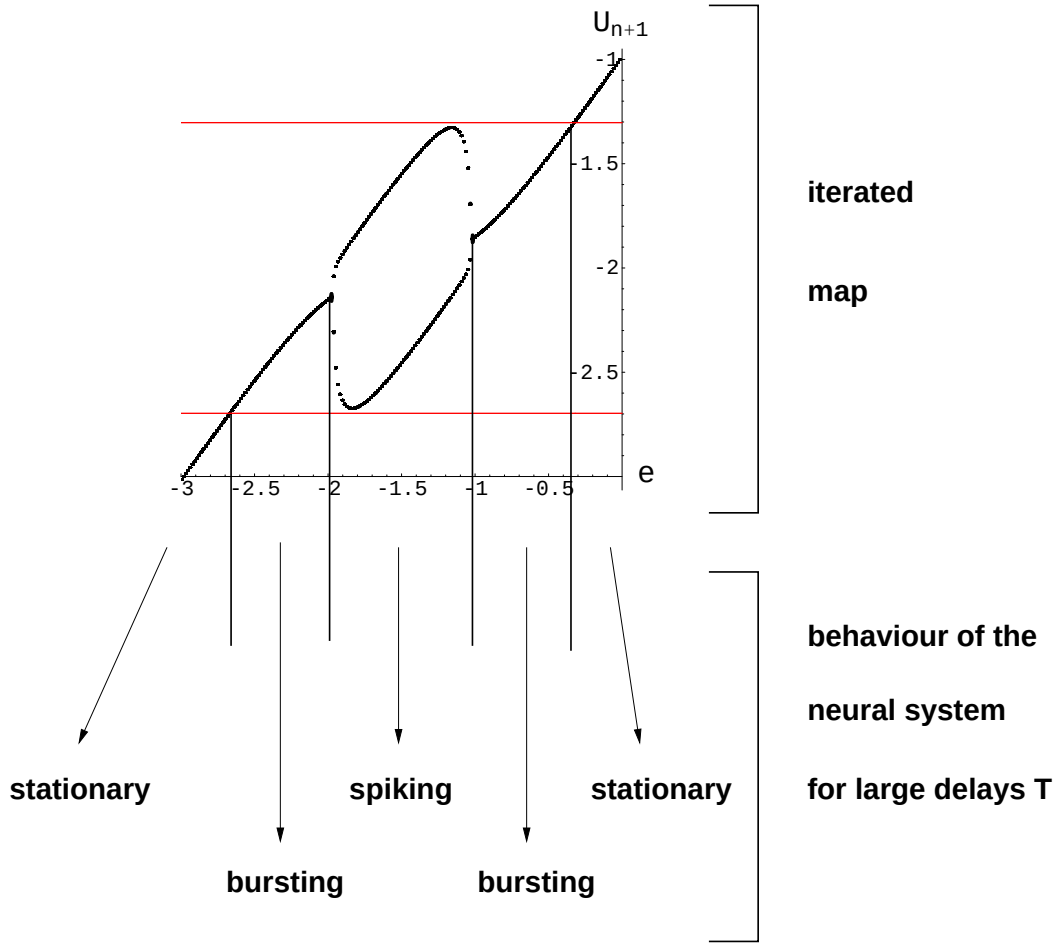

Figure 5.6: The sketch displays the behaviour of the neural system for large time delays T in comparison with the iterated map.

generation of bursting:
Explaining the sketch (figure 5.6) from left to the right we start in the region for the parameter e where the stationary solution of the iterated map lies outside the interval of oscillations of the FitzHugh-Nagumo (FHN) system. In this region the corresponding solutions of the neural system are stationary.
For stationary solutions of the iterated map lying already in the oscillation interval of the FHN system but before the first flip bifurcation the neural system shows bursting.
Parameter values e that correspond to periodic solutions of the iterated map generate spiking in the neural system for large delays.
Values of e that correspond to stationary solutions of the iterated map between the second flip bifurcation point and the upper border of the oscillation interval of the FHN system lead again to bursting in the neural system.
Stationary solutions of the iterated map that lie outside the upper border of the oscillation interval of the FHN oscillator are related to stationary behaviour of the neural system for large delays.
To summarise one can say that bursting in the neuron model for large delays occurs if the bifurcation parameter e corresponds to a stationary solution of the iterated map that lies in the interval of oscillation of the FitzHugh-Nagumo oscillator.
To conclude we would like to show two numerical simulations that were taken out of a scan of the range of the parameter e which are the basis for establishing our theory of the reasons of bursting. Figure 5.7 shows the bursting behaviour of the neural system for the parameter $e = -2.3$ and for time delay $T = 10000$. The spiking region is shown in figure 5.8 for time delay $T = 10000$ and parameter value $e = -1.4$.

5.4 Bursting for small delay

Regarding small delays in the neuron model it was not possible to use the iterated map as an argument. So in this case we had to look at the results of the numerical bifurcation analysis of our system. The stability analysis of the branch of periodic solutions revealed that there exists a part of the branch that is stable and another part that shows an unstable behaviour. With the help of the Floquet multipliers it was possible to find the parameter value e for which the transition between the unstable and the stable part of the branch occurs. Inserting this parameter into the numerical calculations of the solutions of the neuron model, carried out with XPPAUT, also yields the transition point e_{trans} from bursting to spiking, see figure 4.13. Bursting occurs for the unstable and spiking for the stable region of the branch.

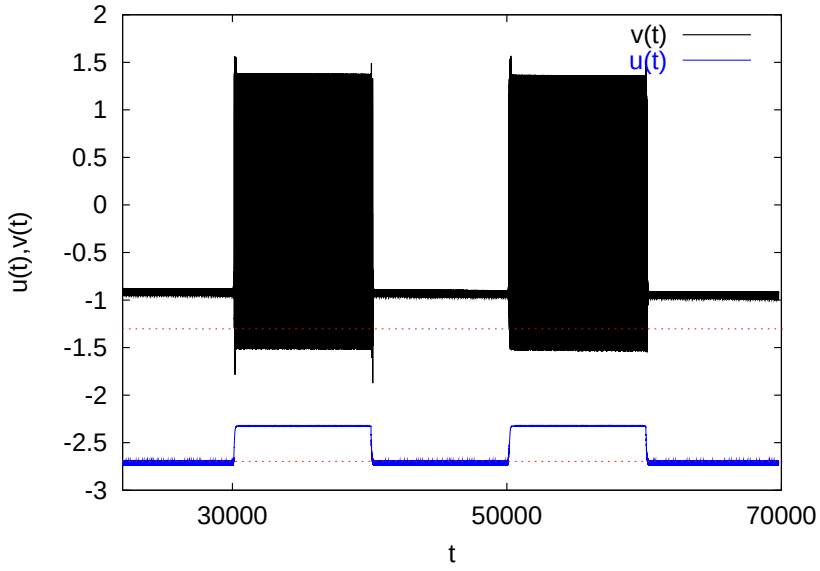

Figure 5.7: Bursting: The figure displays the solutions v(t) (black line) and u(t) (blue line) of the neural system for large time delays $T = 10000$ and for the parameter value $e = -2.3$ calculated with XPPAUT. In addition the borders of the oscillation interval of the FitzHugh-Nagumo oscillator are plotted by red dots.

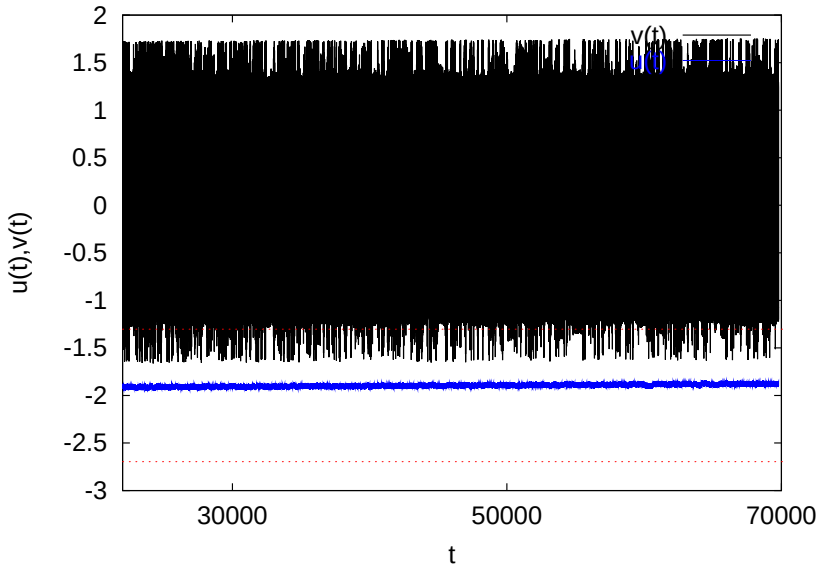

Figure 5.8: Spiking: The figure displays the solutions v(t) (black line) and u(t) (blue line) of the neural system for large time delays $T = 10000$ and for the parameter value $e = -1.4$ calculated with XPPAUT. In addition the borders of the oscillation interval of the FitzHugh-Nagumo oscillator are plotted by red dots.

5.5 Mechanisms of bursting

In summary the mechanisms of bursting can be described for two cases.

- Regarding small time delays numerical calculations lead to the conclusion that bursting corresponds to the unstable part of the branch of periodic solutions and spiking can be seen for the stable part of the branch of periodic solutions. Picking out the branch point at which the transition between unstable and stable periodic solutions occurs facilitates the calculation of the corresponding transition value of the parameter e_{trans}. Bursting then occurs for parameter values of e that lie between the Hopf point of the neuron system and the transition point e_{trans}.

- For large time delays T bursting occurs for parameter values e that correspond either to the region between the lower boundary of the oscillation interval of the FitzHugh-Nagumo system and the first flip bifurcation point e_1^{flip} of the iterated map or between the second flip bifurcation point e_2^{flip} of the iterated map and the upper boundary of the oscillation interval of the FitzHugh-Nagumo oscillator.

Chapter 6

Multiple time scales

In the neuron model the FitzHugh-Nagumo subsystem represents one time scale and the network equation which describes the postsynaptic potential possesses a second time scale. Adding further network equations to our model enables us to describe several postsynaptic potentials which represent incoming signals. As an example the system below describes two different classes of postsynaptic potentials $u(t)$ within one neuron on the basis of the model

$$\begin{aligned} \tau_1 \dot{u}_1(t) &= -u_1(t) + q_1 g(v(t-T_1)) + e_1, \\ \tau_2 \dot{u}_2(t) &= -u_2(t) + q_2 g(v(t-T_2)) + e_2, \\ \dot{v}(t) &= c(w(t) + v(t) - \frac{1}{3}v^3(t)) + \gamma(u_1(t)+u_2(t)), \\ \dot{w}(t) &= (a - v(t) - bw(t))/c. \end{aligned} \tag{6.1}$$

The postsynaptic potentials may have different delay times T respectively different relaxation times τ. So an application of our neuron model consists in the description of nerve cells with potentials of different time scales which can be found in biological systems.
In the first part of this chapter the basic types of postsynaptic potentials that occur in nature are listed and a short summary of their generation is given. We apply the idea of different time scales to a small but realistic neural network and demonstrate the simulation of different types of postsynaptic potentials on the basis of our neuron model. The variation of the time delay during the simulations leads to an interesting phenomenon: With increasing time delay the solutions of the small neural network display burst multiplets. It has been found that it is possible to also generate burst multiplets with a reduced neural network model. With the help of this reduced model the occurence and shape of burst multiplets and their transition states can definitively put down to the parameter T.
The chapter ends with an example of experimental data that attest that burst multiplets also occur in real neural networks.

6.1 Postsynaptic potentials

Every postsynaptic potential is created by a special reaction between a neurotransmitter and a receptor. The postsynaptic potentials are subdivided into two classes: inhibitory and excitatory postsynaptic potentials. Inhibitory potentials are created by hyperpolarisation as a result of closure of cation ion channels and opening of anion ion channels. Inhibitory postsynaptic potentials are not able to exceed the threshold that is necessary for the generation of action potentials at the axon hillock of the neuron. Excitatory postsynaptic potentials are produced from opening of cation ion channels and the influx of positive ions into the neuron. This leads to a depolarisation of the cell membrane and the exceed of the threshold for generation of new action potentials.
The decay of inhibitory as well as excitatory postsynaptic potentials (IPSP respectively EPSP) is splitted into the categories fast, slow and late slow. Figure 6.1 shows a sketch of the temporal course of postsynaptic potentials that occur in neurons. A detailed description of the classes of postsynaptic potentials and the underlying mechanisms is given in [31].

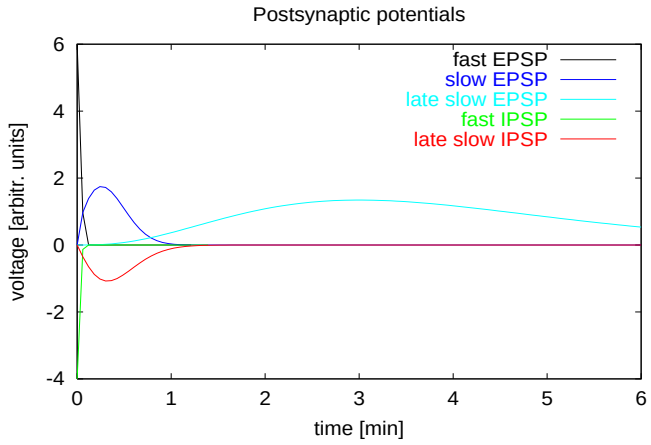

Figure 6.1: Classes of postsynaptic potentials.

6.2 Small neural network consisting of three neurons

A simple and biologically convenient ansatz for the description of different postsynaptic potentials is a system consisting of three coupled neurons, see figure 6.2. It is very unlikely that one neuron has two synapses with itself or with another neuron. We therefore chose the three neuron ansatz to model two different synapses at one neuron. The two inhibitory neurons possess only one synapse

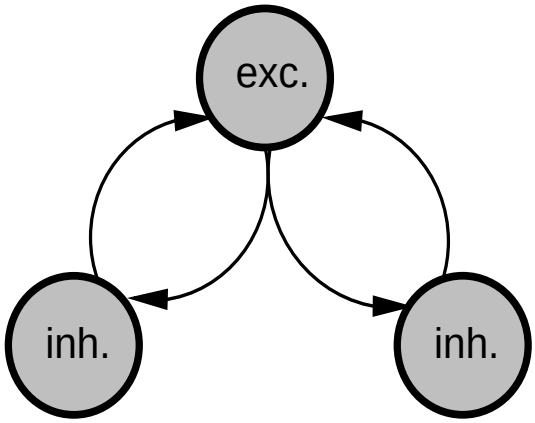

Figure 6.2: Neural network with one excitatory and two inhibitory neurons.

whereas the excitatory nerve cell possesses two synapses. The inhibitory neurons do not have a mutual coupling. The aim of the choice of this three neuron network is the modelling of three classes of postsynaptic potentials: fast IPSP, slow IPSP and a fast EPSP.
The nerve cells of the small neural network in figure 6.2 are described by the following equations. For the excitatory neuron holds

$$\begin{aligned}
\dot{v}^{ex}(t) &= c\{w^{ex}(t) + v^{ex}(t) - \frac{1}{3}(v^{ex})^3(t)\} + \gamma(u_1^{in}(t) + u_2^{in}(t) + e_{ext}^{ex}), \\
\dot{w}^{ex}(t) &= (a - v^{ex}(t) - bw^{ex}(t))/c, \\
\tau_1^{in}\dot{u}_1^{in}(t) &= -u_1^{in}(t) + q^{in}\{g(v_1^{in}(t - T - T^{\delta} - T_1^{\sigma_{in}}))\}, \qquad \text{fast IPSP} \\
\tau_2^{in}\dot{u}_2^{in}(t) &= -u_2^{in}(t) + q^{in}\{g(v_2^{in}(t - T - T^{\delta} - T_2^{\sigma_{in}}))\}. \qquad \text{slow IPSP}
\end{aligned} \tag{6.2}$$

The parameters τ_1 and τ_2 and the coupling constant q are chosen in a way that the last two equations correspond to a fast IPSP and to a slow IPSP. For the two inhibitory neurons we obtain with $k \in \{1, 2\}$

$$\begin{aligned}
\dot{v}_k^{in}(t) &= c\{w_k^{in}(t) + v_k^{in}(t) - \frac{1}{3}(v_k^{in})^3(t)\} + \gamma(u_k^{ex}(t) + e_{ext}^{in_k}), \\
\dot{w}_k^{in}(t) &= (a - v_k^{in}(t) - bw_k^{in}(t))/c, \\
\tau_k^{ex}\dot{u}_k^{ex}(t) &= -u_k^{ex}(t) + q^{ex}\{g(v^{ex}(t - T - T^{\delta} - T_k^{\sigma_{ex}}))\} \qquad \text{fast EPSP}
\end{aligned} \tag{6.3}$$

with τ_k and q providing a fast EPSP in the last equation. The variables and parameters in the three neuron network are defined as follows:

u : postsynaptic potential	v : membrane potential
w : recovery variable	g : neuronal transfer function
q^{in} : inhibitory coupling (negative)	q^{ex} : excitatory coupling (positive)
τ : synaptic time constant	e_{ext} : external signal
T : time delay between neurons	T^{δ}, T^{σ} : dendritic, synaptic time delay
γ : membrane conductance	a, b, c : constants

We take into account delays due to synaptic and dendritic propagation time of the signal and the model contains a general delay T characterising the signal transmission between neurons. In contrast to the neuron model considered in the previous chapters we also allow a membrane conductance γ representing diffusive effects.
The processes of the signal transmission in the three neuron network are illustrated representatively for the excitatory neuron in a flow diagram in figure 6.3. Both inhibitory neurons send their outgoing signal v to the excitatory neuron where it is first transformed by the neuronal transfer function g. Then the signal passes the synapses and is supplied with an inhibitory coupling term q and a delay due to synaptic processes. The effect of the network equation with respect to the synaptic time constant can be regarded as a low pass filter. After an interneural transmission time T^{δ} all postsynaptic signals are summed up and they reach the nonlinear oscillator where an outgoing signal is generated in dependence on the two incoming postsynaptic potentials and the external signal e.

6.3 Burst multiplets

A numerical simulation of the coupled system consisting of (6.2) and (6.3) was performed using XPPAUT, see figure 9.4. Due to the choice of the simulation parameters the excitatory neuron generates a fast excitatory postsynaptic potential which is drawn in red. One inhibitory neuron with a small parameter value of τ displays a fast inhibitory postsynaptic potential which is drawn in black. The second inhibitory neuron provided with a large time constant τ shows slow inhibitory postsynaptic oscillations that are denoted by the blue curve.

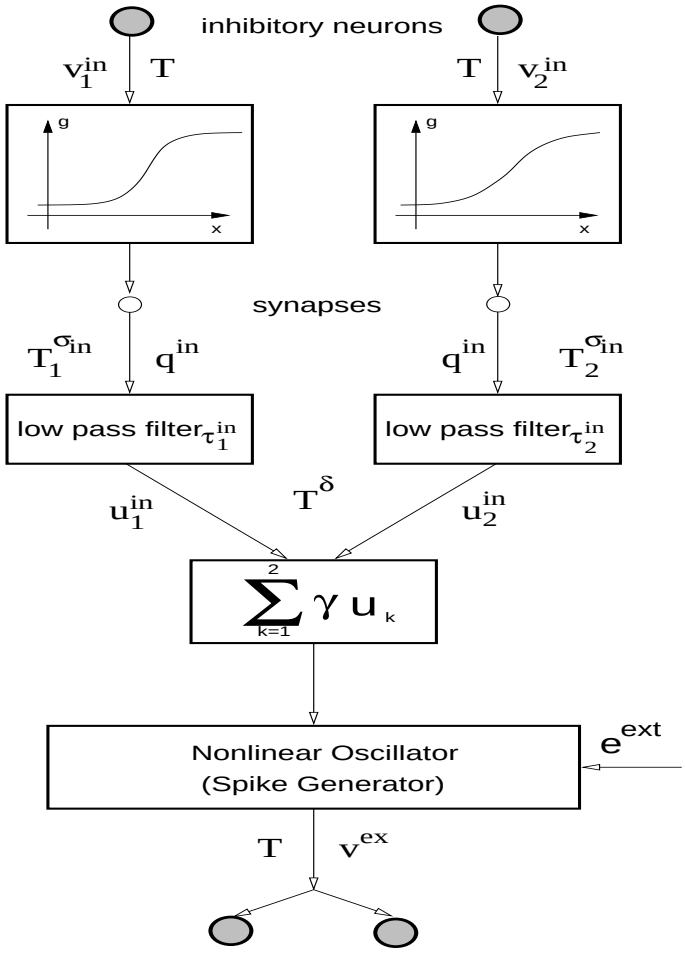

Figure 6.3: Flow diagram of the excitatory neuron.

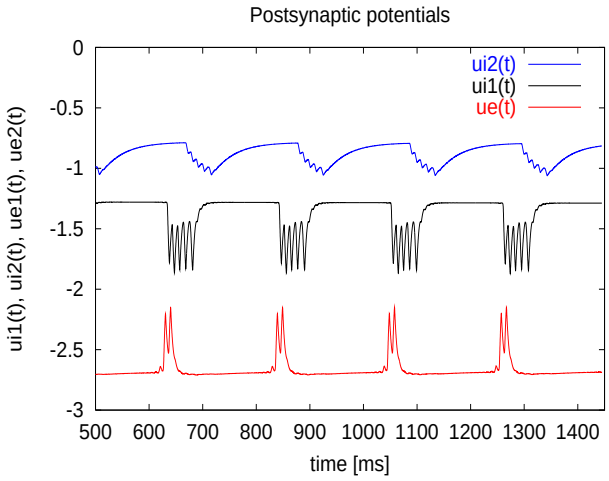

Figure 6.4: Different classes of modelled postsynaptic potentials. The blue potential (ui2) corresponds to a slow inhibitory postsynaptic potential, the black curve (ui1) shows a fast inhibitory postsynaptic potential and the red curve (ue=ue1=ue2) denotes a fast excitatory postsynaptic potential.

The parameter set used for this simulation is

$$\begin{aligned} \tau_1^{in} &= 5 \text{ ms} & T + T^{\delta} + T_1^{\sigma_{in}} &= 5 \text{ ms} \\ \tau_2^{in} &= 40 \text{ ms} & T + T^{\delta} + T_2^{\sigma_{in}} &\text{ varies} \\ \tau_k^{ex} &= 5 \text{ ms} & T + T^{\delta} + T_k^{\sigma_{ex}} &= 5 \text{ ms} \\ q^{ex} &= 1.0 & q^{in} &= -1.0 \\ a = b &= 0.9 & c &= 2 \\ e_{ext}^{ex} &= -2.5074 & e_{ext}^{in_k} &= -2.725 \\ \gamma &= 1. \end{aligned}$$

With increasing time delay of the slow inhibitory postsynaptic potential an interesting effect occurs: Burst multiplets are created in dependence on the time delay. Results of the three neuron network show that the prerequisite for the generation of burst multiplets is that both inhibitory synapses differ with regard to the synaptic time constant and synaptic time delay. This means that one synapse generates a fast and the other a slow postsynaptic potential. The postsynaptic potentials and the membrane potentials of all three neurons in our small network are shown in figure 6.5 in dependence on the parameter $T_2^{\sigma_{in}}$. For $T_2^{\sigma_{in}} = 35\ ms$ we obtain the classes of postsynaptic potentials described above. With increasing time delay new structures are generated and for $T_2^{\sigma_{in}} = 125\ ms$ the neural network displays oscillations in the form of burst doublets. A further increase of the time delay to $T_2^{\sigma_{in}} = 180\ ms$ generates burst triplets.

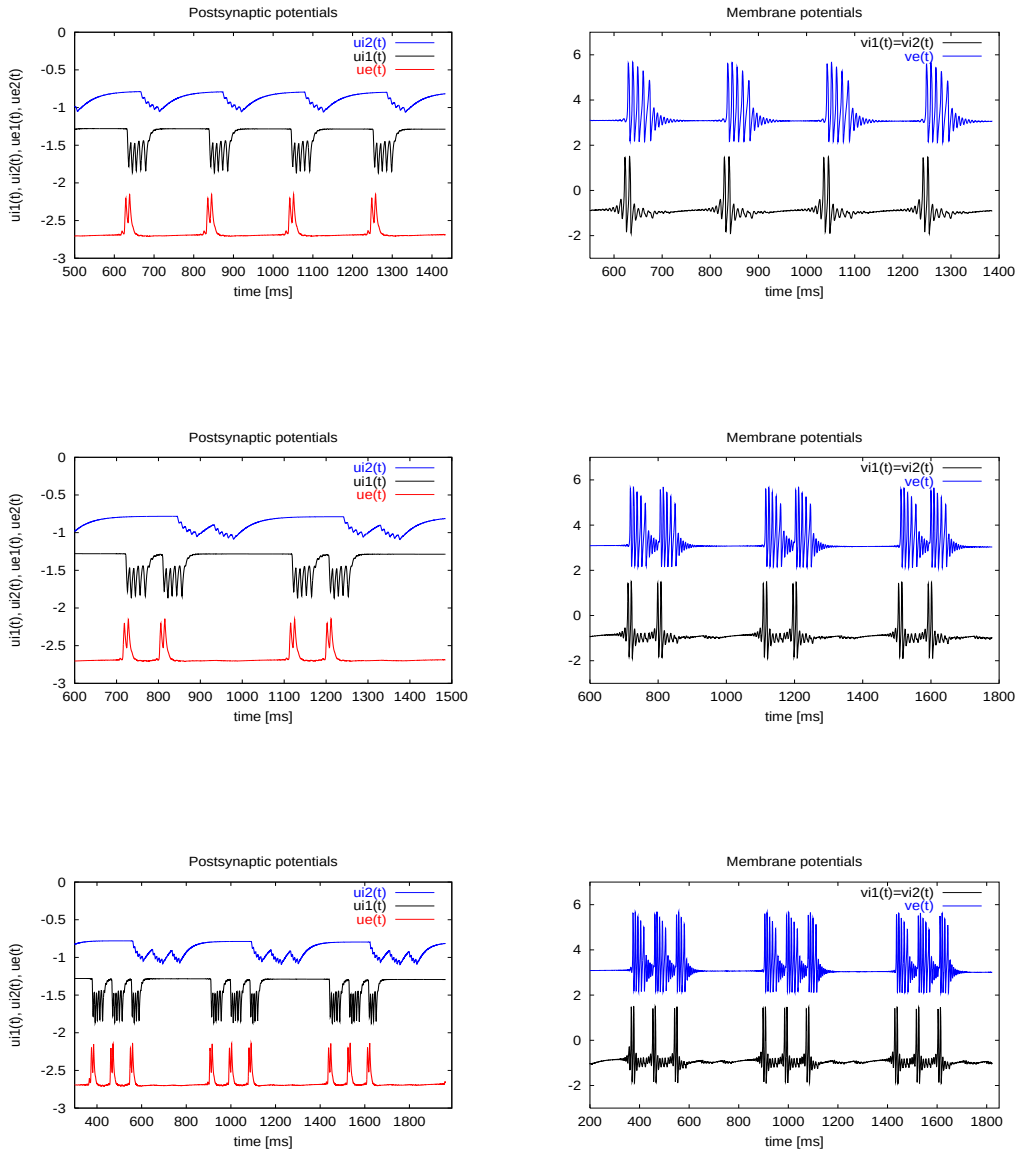

Figure 6.5: Generation of burst multiplets in the postsynaptic potential and in the membrane potential of the three neuron system.
Top: simulations for $T_2^{\sigma_{in}} = 35\,ms$, middle: simulations for $T_2^{\sigma_{in}} = 125\,ms$, bottom: simulations for $T_2^{\sigma_{in}} = 185\,ms$.

6.4 Reduction of the model

The formation of burst multiplets shown in the previous section can not be well studied in a large system like the three neuron network. We therefore looked for a reduction of the three neuron model that still produces burst multiplets. As mentioned above the superposition of different delays is responsible for the generation of burst multiplets. So the simplest model for burst multiplets is the basic neuron model with two incoupled potentials v that have different time delay. Especially the time delay of one membrane potential v can be equal to zero.

$$\begin{aligned} \tau\dot{u}(t) &= -u(t) + q\{g(v(t)) + g(v(t-T))\} + e, \\ \dot{v}(t) &= c(w(t) + v(t) - \frac{1}{3}v^3(t)) + \gamma u(t), \\ \dot{w}(t) &= (a - v(t) - bw(t))/c. \end{aligned} \tag{6.4}$$

System (6.4) contains only three time scales: the fast subsystem of the FitzHugh-Nagumo oscillator and the slow subsystem of the network equation which possesses two time scales due to one delayed and one non delayed membrane potential.
Equation (6.4) was analysed numerically and its solutions are plotted for different values of delay T (figure 6.6). For $T = 50\ ms$ the solution displays periodic bursting and a Fourier analysis of the frequencies shows that there are some main oscillation frequencies that are responsible for the periodic bursting.

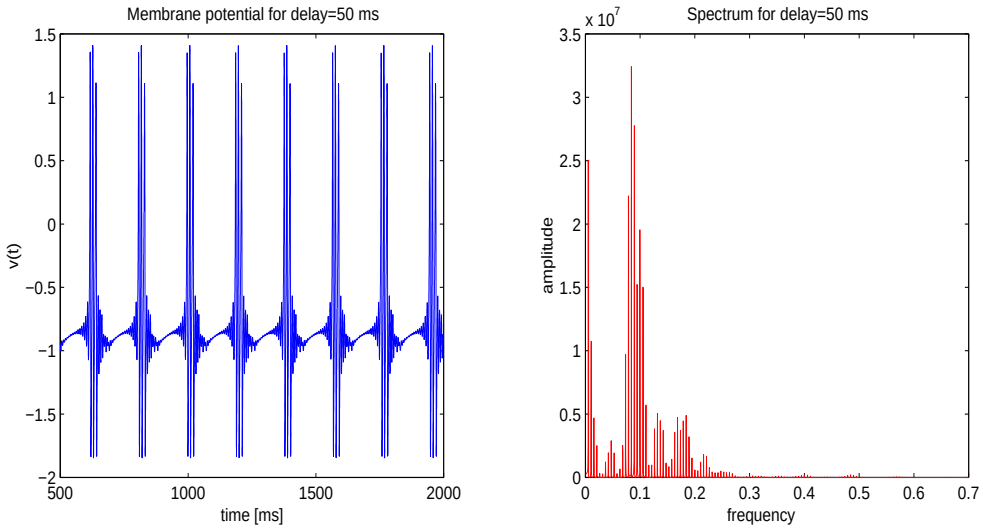

Figure 6.6: Simulations of the reduced model for $T = 50\ ms$. Left: membrane potential. Right: frequency spectrum.

The corresponding phase portrait in figure 6.7 as well as the frequency analysis in figure 6.6 indicate that the solution for $T = 50\ ms$ behaves almost non chaotic.

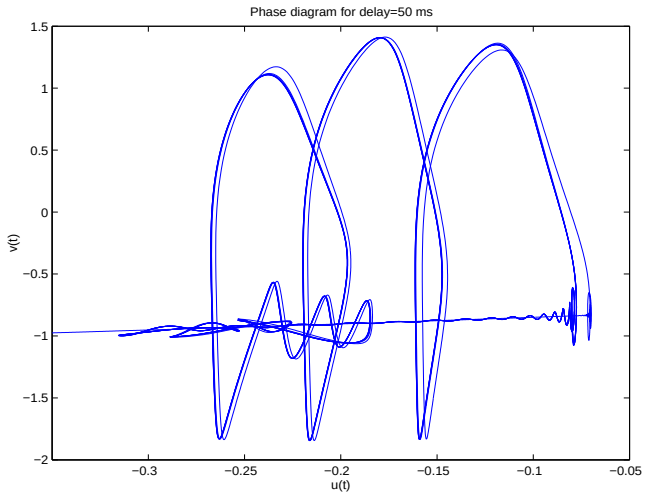

Figure 6.7: Phase diagram for $T = 50\ ms$.

An increase of the time delay to $T = 80\ ms$ in system (6.4) leads to a transition state between regular bursting and a burst doublet. Here the transition state displays a wide spectrum of frequencies and a chaotic structure of the phase diagram (see figures 6.8 and 6.9).
At $T = 110\ ms$ the superposition of the three time scales yield the generation of burst doublets, see figure 6.10. The frequencies are less wide spread than in the transition state at $T = 80\ ms$. The corresponding phase diagram is shown in figure 6.11.
A further increase of the time delay T leads to the generation of burst multiplets containing three bursts et cetera.
The study of the neural model consisting of three time scales reveals that there occurs a bifurcation of the number of bursts per multiplet with respect to the bifurcation parameter T.
Periodic oscillations in the form of bursting are a widespread phenomenon in neurons. But also the formation of burst doublets and burst triplets can be observed in real neural networks. An example of burst multiplets is described in [34]. Here the cells of the brain stem of tadpoles are analysed in order to obtain informations on gill and lung ventilation in pre- and postmetamorphic states. Recordings of the tadpole brain stem are shown in figure 6.12 and in figure 6.13.

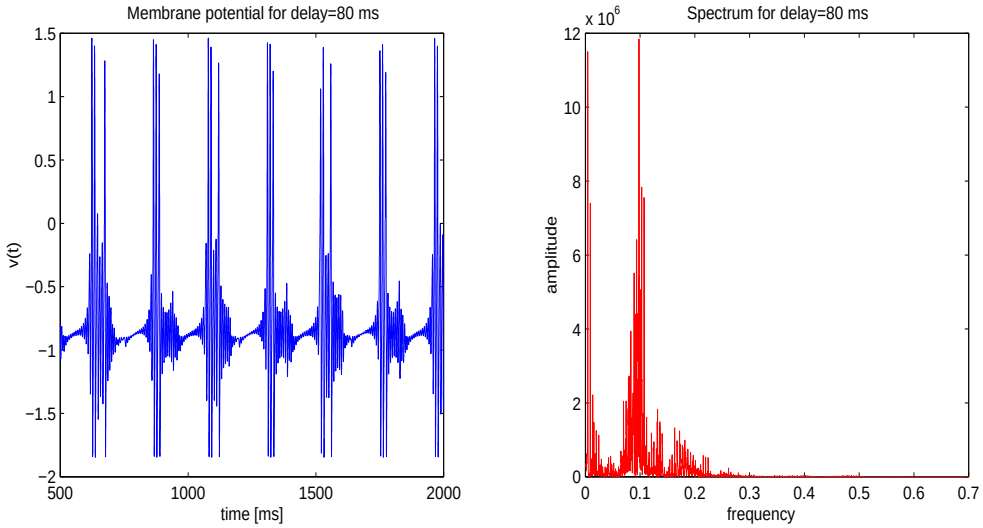

Figure 6.8: Simulations of the reduced model for $T = 80\ ms$. Left: membrane potential. Right: frequency spectrum.

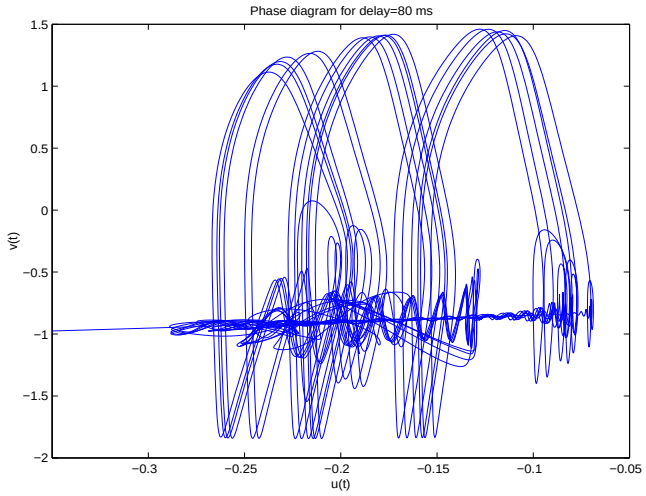

Figure 6.9: Phase diagram for $T = 80\ ms$.

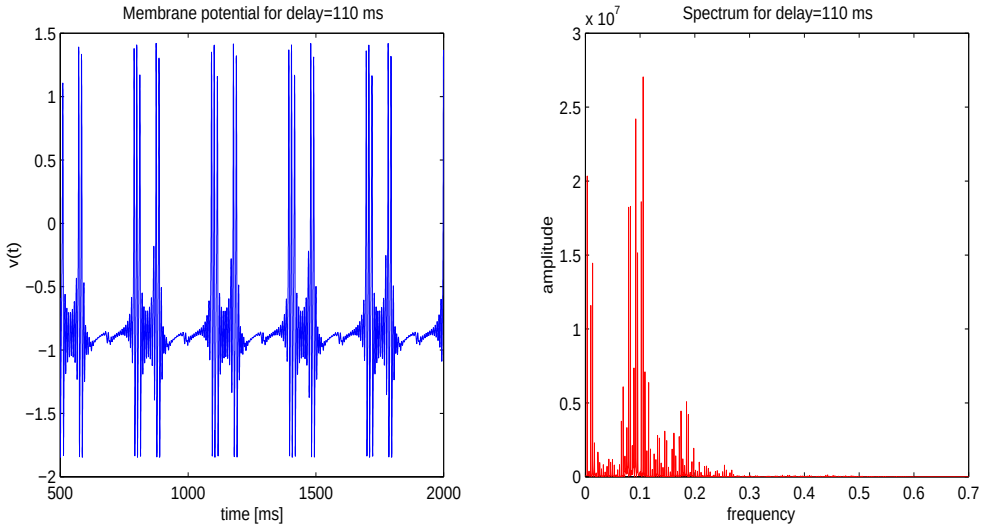

Figure 6.10: Simulations of the reduced model for $T = 110\ ms$. Left: membrane potential. Right: frequency spectrum.

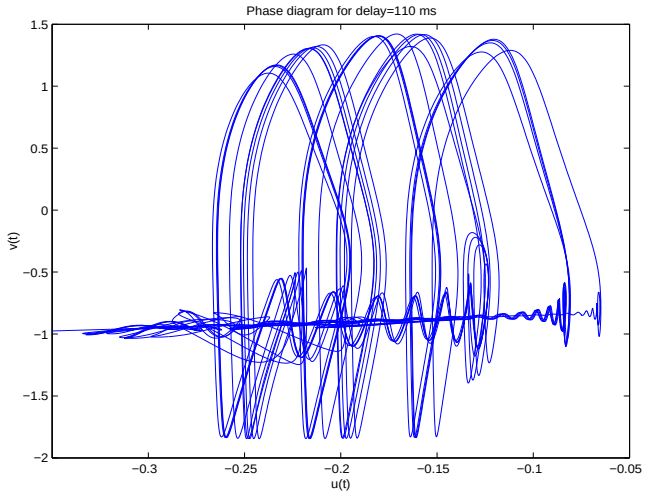

Figure 6.11: Phase diagram for $T = 110\ ms$.

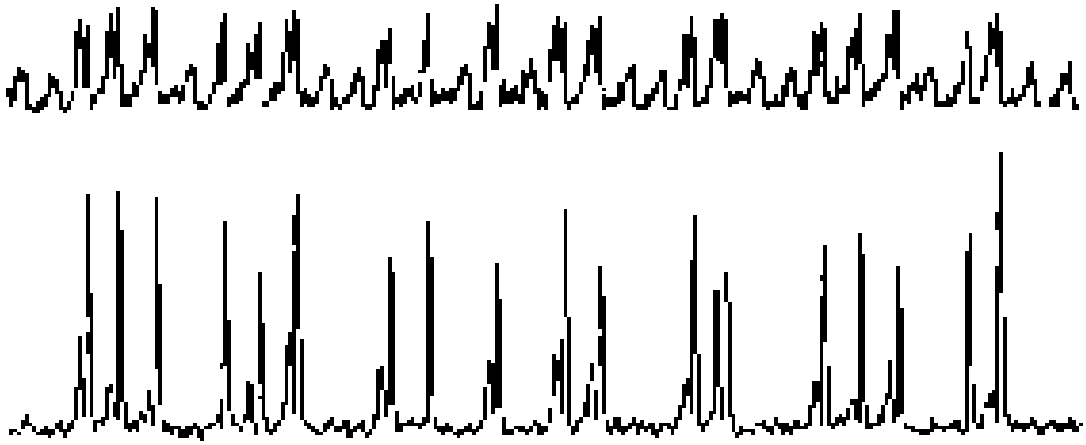

Figure 6.12: Burst multiplets in the cells of the tadpole brain stem (taken from [34]).

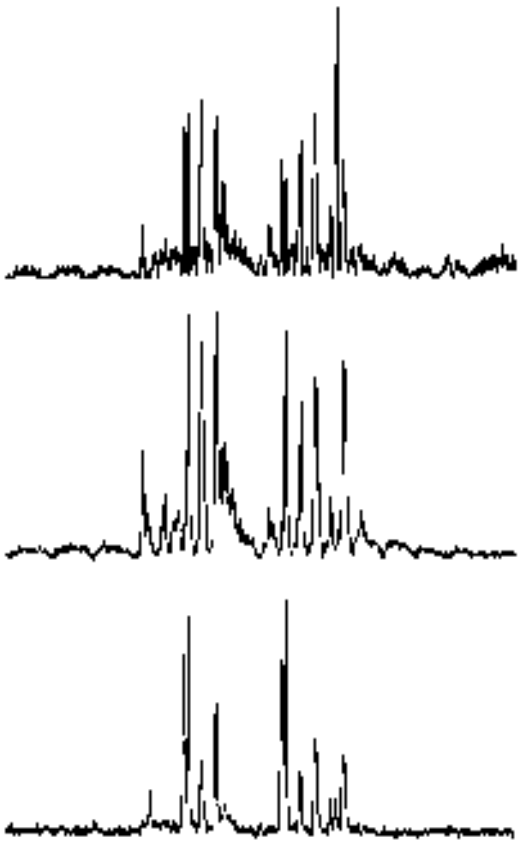

Figure 6.13: Burst doublets in the tadpole brain stem (taken from [34]).

Chapter 7

Prospects

It is the aim of this chapter to shortly present some aspects of the neuron model and the bifurcation analysis that could not be investigated in this thesis but whose analysis seems to be rewarding.

As mentioned in chapter 4 and 5 it turned out that DDE-BIFTOOL has difficulties to follow a branch of periodic solutions in the case of large delays and in the case of systems that obtain different time scales. It would be worth focussing on this problem and making use of all numerical features of DDE-BIFTOOL in order to clarify whether this is a principal problem of DDE-BIFTOOL or only a problem of the chosen numerical routines and related parameters.

In order to obtain an overall impression of the neuron model it would be very useful to analyse its bifurcation behaviour numerically in dependence on all important system parameters. Analytical methods similar to those already presented in chapter 2 and 3 could supply the numerical results and could be used as reference results in order to avoid numerical artefacts.

The coupling between pre- and postsynaptic potentials in the neuron is modelled by the coupling constant q. The coupling between network equation and FitzHugh-Nagumo subsystem however has been regarded up to now as constant. Introducing a diffusive coupling constant γ into the neuron model

$$\begin{aligned} \tau\dot{u}(t) &= -u(t) + qg(v(t-T)) + e, \\ \dot{v}(t) &= c(w(t) + v(t) - \frac{1}{3}v^3(t)) + \gamma\, u(t), \\ \dot{w}(t) &= (a - v(t) - bw(t))/c \end{aligned}$$

and analysing its influence on the system could lead to a more realistic model of the neuron.
A further extension of our system could be the introduction of time dependent external signals $e(t)$.

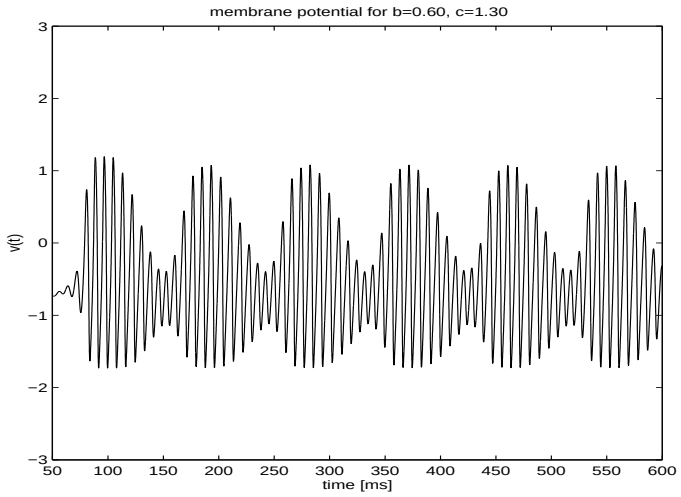

Figure 7.1: Waxing and waning membrane potential of the neuron due to supercritical Hopf bifurcation in the underlying FitzHugh-Nagumo system.

To demonstrate an example of the properties of the model worth to be analysed we present a possible application of our neuron model to spindle oscillations in the thalamus [5, 33, 4]. Spindle oscillations consist of waxing and waning potentials that are separated by long rest periods. Typically spindles occur at the beginning of sleep. They are put down to complex mechanisms in the cells. Spindle oscillations as well as the related brain area are well investigated and experimental data suggest that epileptic seizures are generated by mechanisms that are similar to those that generate spindle oscillations.
In order to model waxing and waning oscillations with the neuron model used in this thesis we will present shortly two possible methods. First an application of an appropriate, time-dependent external signal $e(t)$ can generate waxing and waning oscillations. A second method uses the properties of the FitzHugh-Nagumo system: In the case of a supercritical Hopf bifurcation that holds for $\frac{1}{2} < b < 1$, $b < c^2 < \frac{b^2}{2b-1}$ (see [14] for further details) the transition to periodic solutions is soft which leads to waxing and waning oscillations for our neuron model (see figure 7.1). The open task in this problem is to find conditions for which the waxing and waning solutions become separated by long quasistationary regions.

Chapter 8

Conclusion

Basis of the investigations within this thesis is a neuron model describing the membrane potentials as well as the postsynaptic potentials of a neuron. The neuron is modelled by a coupled system of three differential equations with delay. It consists of a FitzHugh-Nagumo oscillator that is to be considered as an oscillation generator at the axon hillock of the neuron. Further, the model consists of a network equation that sums up all incoming signals and describes the synaptic properties of the neuron. The solutions of the neuron model display three different types of dynamics: stationary behaviour, bursting and spiking. Bursting is characterised by periodic oscillations that are separated by phases of quasistationary behaviour. Permanent oscillations however are called spiking. The different types of dynamics depend on the parameters of the neuron model. Bursting up to now has been regarded as a phenomenon that arises due to the interaction of different time scales within the model. Parameter values that lead to bursting were obtained empirically.
It was the aim of this thesis to find a connection between the appearance of bursting and the bifurcation properties of the neuron model.
For this purpose the neuron model was analysed using three different approaches. These were the analysis of the complete system for the limiting case of infinite delay time T of the model, the analysis of the stability of the stationary solutions of the model for finite and infinite delay and a bifurcation analysis of the complete system using a numerical bifurcation tool for delay differential equations.
In the following a deeper insight into the three approaches is given.

First approach

For the limiting case of infinite delay time T it was possible to derive an iterated map from the equations of the neuron model. The iterated map was analysed numerically which led to a bifurcation diagram that displayed stationary solutions as well as a range of periodic solutions in dependence on the bifurcation parameter e. In the model e represents an external signal to the network equa-

tion. Biologically this signal is collected at the synapse of the neuron.
With the numerical analysis the type of bifurcation was determined to be a flip bifurcation of the iterated map.
Applying analytical methods with regard to flip bifurcations we determined for which values of e the transition between stationary and periodic behaviour of the iterated map occured.

Second approach

As a second step the bifurcation properties of the neural system were examined by an analysis of the stability of the stationary solutions of the model. For this purpose a result of Giannakopoulos et al. [14] was used which yields the transition points between stable stationary and unstable stationary behaviour in dependence on the parameters e and the coupling constant q between membrane potential and postsynaptic potential.
The loss of stability of the stationary solutions was then calculated again for the limiting cases $T \to \infty$ and $\tau \to \infty$ (τ denotes the relaxation time of the postsynaptic potential).
In the case of $T \to \infty$ the transition points between stable stationary and unstable stationary regions turned out to be exactly the flip bifurcation points of the iterated map.
In the case of $\tau \to \infty$ the equations of the system decouple. That means that the postsynaptic potential becomes stationary and the FitzHugh-Nagumo system with the postsynaptic potential u as bifurcation parameter remains. The bifurcation behaviour of the FitzHugh-Nagumo system is well documented in literature [12, 17, 24, 35].

Third approach

Using the numerical bifurcation tool DDE-BIFTOOL a bifurcation analysis of the complete system was performed. DDE-BIFTOOL proceeds in analysing delay differential systems as follows: Emanating from the stationary solution bifurcation points were searched in dependence on e. If bifurcation points were found the type of bifurcation can be determined. For our model two Hopf bifurcation points were detected which correspond exactly to the transition points between stable stationary and unstable stationary solutions given in approach two in the case of finite delay. Starting at the bifurcation point a branch of periodic solutions can be followed. In addition the stability of the periodic solutions can be determined for each point located on the branch. Stable as well as unstable parts of the branch of periodic solutions were found.
The bifurcation analysis was also performed for a large time delay. Here the resulting bifurcation points are equal to those obtained for the iterated map.

Regarding each approach by itself leads to interesting results but within the frame of this thesis it was important to compare the three methods and study the correlations between them in order to obtain a deeper insight into the mechanisms responsible for bursting.
For finite delay it turned out that there is no difference between the potential Hopf bifurcation points of the neuron model obtained by analysing the stability of stationary solutions and the Hopf bifurcation points calculated with DDE-BIFTOOL. That means that with the help of analytical calculations it is possible to check the results of DDE-BIFTOOL which for systems with different time scales like our system sometimes displays difficulties in producing reliable results. The bifurcation results of the iterated map and the analysis using DDE-BIFTOOL can also be compared. For this purpose one has to choose a large delay time for DDE-BIFTOOL because the iterated map only yields results for infinite delay. Although the delay times are not equal and DDE-BIFTOOL has difficulties in calculating the branches of periodic solutions for large time delay and the way to find the bifurcations is different in both cases the same bifurcation points were found.
In addition, solutions of the neuron model for large time delay T were calculated with XPPAUT, a software that solves delay differential equations. The obtained solutions displaying stationary behaviour, bursting or spiking in dependence on e were compared with the iterated map. Calculations yield that the periodic region of the iterated map for the variable U lies completely within the oscillation interval of the FitzHugh-Nagumo oscillator. Now the comparison of solutions of the neuron model for large time delays T yields that bursting corresponds to special regions for the values of e. These regions are characterised by the iterated map displaying stationary behaviour and lying within the oscillation interval. In contrast spiking occurs for values of e that are related to the periodic solutions of the iterated map. For all other values of e the neural system is stationary.
In the case of small delays it is not possible to refer to the iterated map. So one has to take the results of the DDE-BIFTOOL analysis of the branch of periodic solutions. The numerical calculations showed that for e corresponding to the unstable part of the branch the solutions of the neuron model display bursting. Spiking on the other hand refers to the stable part of the branch of periodic solutions.

Finally in this thesis the neuron model was used to describe qualitatively the behaviour of postsynaptic potentials of nerve cells. The idea of different time scales was applied to a small but realistic neural network of three neurons which made it possible to model different types of postsynaptic potentials. For well

chosen e the time delay turned out to be a parameter which is responsible for the occurence of burst multiplets and the number of bursts within one multiplet. With increasing time delay the number of bursts in a multiplet grows. Since the formation of burst multiplets could not be well studied in the large model of the three neuron network the model was reduced to a simpler model that still generated burst multiplets. This system was analysed numerically. We found that with increasing number of bursts in a multiplet the system showed a more complex structure of the phase diagrams.
The phenomenon of burst multiplets which was found in context with the modelling of postsynaptic potentials of nerve cells has also a counterpart in biology. Recordings of the brain stem of tadpoles in order to analyse pre- and postmetamorphic states of gill and lung ventilation for example display burst multiplets.

Chapter 9

Zusammenfassung

9.1 Bursting in Modellen mit Zeitverzögerung für neuronale Netze

In der vorliegenden Arbeit werden Mechanismen, die zu Bursting in einem Neuronenmodell führen, untersucht. Als Bursting wird eine Oszillationsform der Potentiale von Nervenzellen bezeichnet, die sich durch Phasen periodischer Aktivität auszeichnet. Zwischen den Phasen periodischer Aktivität zeigt sich quasistationäres Verhalten. Eine weitere Oszillationsart von Nervenzellen ist Spiking, das ein kontinuierliches Oszillieren des Potentials bezeichnet.
In bisherigen Veröffentlichungen wurden für das Auftreten von Bursting empirisch gefundene Kriterien angegeben. Das heißt, dass aus numerischen Simulationen Parameterbereiche abgeleitet wurden, für die Bursting auftritt. Ziel dieser Arbeit ist es, Kriterien für das Auftreten von Bursting zu finden, die sich direkt aus den Verzweigungseigenschaften des Modells herleiten lassen.

9.1.1 Mathematisches Modell

Das Neuronenmodell, das in dieser Arbeit untersucht wird, besteht aus drei gekoppelten nichtlinearen Differentialgleichungen mit Zeitverzögerung T.

$$\begin{aligned} \tau\ddot{u}(t) &= -u(t) + qg(v(t-T)) + e, \\ \dot{v}(t) &= c(w(t) + v(t) - \frac{1}{3}v^3(t)) + u(t), \\ \dot{w}(t) &= (a - v(t) - bw(t))/c. \end{aligned}$$

Die Variable u beschreibt das postsynaptische Potential einer Nervenzelle. Es setzt sich aus allen Signalen zusammen, die an der Synapse eingehen und dort je nach Art der Synapse entweder mit einer inhibitorischen (negativen) oder einer exzitatorischen (positiven) Kopplung q versehen werden. Eine wichtige Eigenschaft der postsynaptischen Potentiale ist ihre Abklingzeit. Diese wird in un-

serem Modell durch den Parameter τ modelliert. Zusätzlich berücksichtigt werden außerdem externe konstante Signale e, die ebenfalls in das postsynaptische Potential eingehen.
Das ausgehende Signal einer Nervenzelle wird am Axonhügel erzeugt. Im vorliegenden Modell entspricht das dem FitzHugh-Nagumo Untersystem, das aus den Variablen v und w besteht. v ist das ausgehende Signal oder auch Membranpotential und w ist eine Hilfsvariable.

9.1.2 Verzweigungsanalyse

Um Kriterien für das Auftreten von Bursting zu finden, die auf der Parameterabhängigkeit des Modells beruhen, müssen die Verzweigungseigenschaften des neuronalen Systems untersucht werden. Dies ist schwierig, da es sich um ein dreidimensionales, nichtlineares System handelt, das eine Zeitverzögerung beinhaltet. Deshalb werden drei verschiedene Wege gewählt, um Verzweigungseigenschaften berechnen zu können. Die Kombination der Ergebnisse dieser Ansätze ermöglicht es dann, Bedingungen anzugeben, für die Bursting in Abhängigkeit vom Verzweigungsparameter e auftritt. Die verschiedenen Herangehensweisen werden im Folgenden kurz dargestellt.

Iterierte Abbildung

Zunächst wird der Fall unendlicher Zeitverzögerung untersucht. Das mathematische Modell für ein Neuron kann dann in Form einer iterierten Abbildung beschrieben werden. Die Darstellung der iterierten Abbildung für die Variable U ist durch

$$U_{n+1} = qg(H^{-1}(U_n)) + e$$

gegeben. Die verwendete Hilfsfunktion lautet

$$H(V(s)) := c(\frac{1}{3}V^3(s) + V(s)(\frac{1}{b} - 1) - \frac{a}{b}) = U(s).$$

Die explizite Darstellung ihrer inversen Funktion $H^{-1}(U(s))$ ist im Anhang B aufgeführt. Eine numerische Verzweigungsanalyse der iterierten Abbildung ergibt, dass es in Abhängigkeit vom Parameter e sowohl stationäre als auch periodische Lösungen der iterierten Abbildung gibt (siehe Abbildung 9.1). Der Übergang zu den periodischen Lösungen erfolgt als superkritische Flip-Verzweigung der iterierten Abbildung. Mit Hilfe von analytischen Methoden wurden die beiden Flip-Ver-
zweigungspunkte bestimmt und die Verzweigungsrichtung bestätigt. Die beiden Flip-Verzweigungspunkte wurden für den Parametersatz $(a, b, c, q) = (0.9,\ 0.9,\ 2.0,\ -1.0)$ berechnet zu:

$$e_1^{flip} = -1.97 \qquad\qquad e_2^{flip} = -1.03.$$

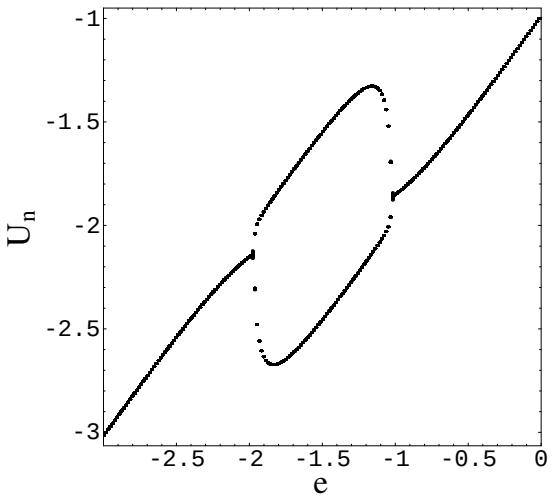

Figure 9.1: Iterierte U-Abbildung in Abhängigkeit vom Verzweigungsparameter e.

Stabilitätsanalyse für stationäre Lösungen

Die Verzweigungseigenschaften des Neuronenmodells werden im zweiten Ansatz mittels einer Stabilitätsanalyse der stationären Lösung des Systems untersucht. Ausgehend von Ergebnissen von Giannakopoulos et al. [14], die potentielle Hopf-Punkte in Abhängigkeit von den Parametern e und q liefern, wird der Stabilitätsverlust der stationären Lösung für die beiden Grenzfälle $T \to \infty$ und $\tau \to \infty$ untersucht. Im Falle unendlicher Zeitverzögerung ergeben sich exakt die Verzweigungspunkte, die in der Analyse der Flip-Verzweigung der iterierten Abbildung berechnet wurden. Der Grenzfall $\tau \to \infty$ führt dagegen zu einer Entkopplung des Systems. Die Dynamik wird dann nur noch durch den FitzHugh-Nagumo Oszillator bestimmt, wobei das postsynaptische Potential u als Verzweigungsparameter dient.

Numerische Verzweigungsanalyse

Eine numerische Verzweigungsanalyse des Neuronenmodells wurde mit Hilfe des Matlab Paketes DDE-BIFTOOL erstellt. Diese Sammlung numerischer Routinen für zeitverzögerte Differentialgleichungen ermöglicht die Berechnung von Verzweigungspunkten und die Fortsetzung von periodischen Lösungen.
Für das Neuronenmodell wurden zwei Hopf-Verzweigungspunkte gefunden, und durch Berechnen des Zweiges der periodischen Lösungen wurde das Verzweigungsdiagramm für die Variable v in Abhängigkeit vom Verzweigungsparameter e erstellt (siehe Abbildung 9.2). Desweiteren wurde die Stabilität auf dem Zweig der

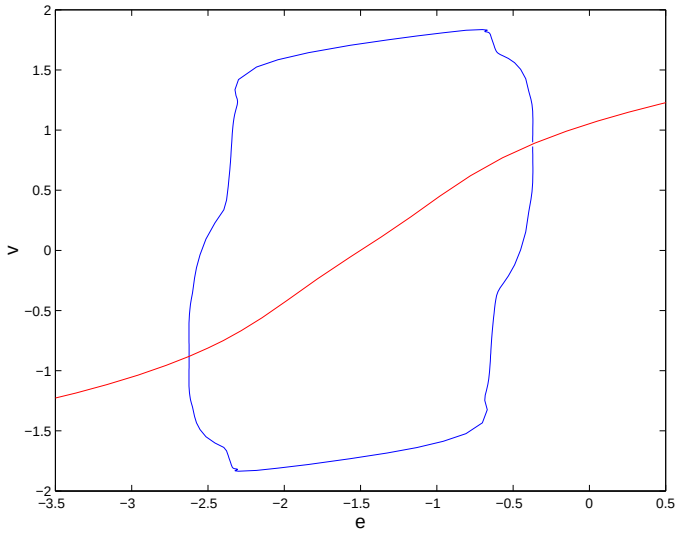

Figure 9.2: Verzweigungsdiagramm des Membranpotentials v in Abhängigkeit vom Verzweigungsparamter e. Die rote Linie stellt die stationäre Lösung dar und die Einhüllende der periodischen Lösung ist in blau aufgetragen.

periodischen Lösungen mit Hilfe der Floquet-Multiplikatoren bestimmt. Eine Untersuchung des Modells für sehr große Zeitverzögerungen schließt die numerische Verzweigungsanalyse ab.

9.1.3 Ergebnisse der Verzweigungsanalyse

Vergleich der Verzweigungseigenschaften

Für endliche Zeitverzögerungen wird durch die numerische Verzweigungsanalyse mit DDE-BIFTOOL bestätigt, dass es sich bei den potentiellen Hopf-Punkten, die aus dem Ansatz des Stabilitätsverlustes der stationären Lösung berechnet werden, tatsächlich um solche handelt.
Im Falle unendlicher bzw. sehr großer Zeitverzögerung können die Resultate der iterierten Abbildung und der numerischen Verzweigungsanalyse für große Zeitverzögerungen miteinander verglichen werden. In beiden Fällen wurden die gleichen Parameterwerte für die Verzweigungspunkte gefunden.
Ein weiteres Ergebnis dieser Arbeit ist die Erkenntnis, dass mit Hilfe analytischer Methoden und mit der Simulation der Lösungen des Neuronensystems unter Verwendung der Software XPPAUT Kontrollrechnungen für das Verzweigungsverhalten möglich sind. Dies erweist sich als wichtig, da das DDE-BIFTOOL bei der Berechnung von Zweigen periodischer Lösungen für Systeme mit mehreren Zeitskalen und für sehr große Zeitverzögerungen aufgrund numerischer Schwierigkeiten an seine Grenzen stößt.

Mechanismen für Bursting

Aus den Resultaten für die verschiedenen Ansätze zur Verzweigungsanalyse lassen sich folgende Kriterien für das Auftreten von Bursting ableiten.

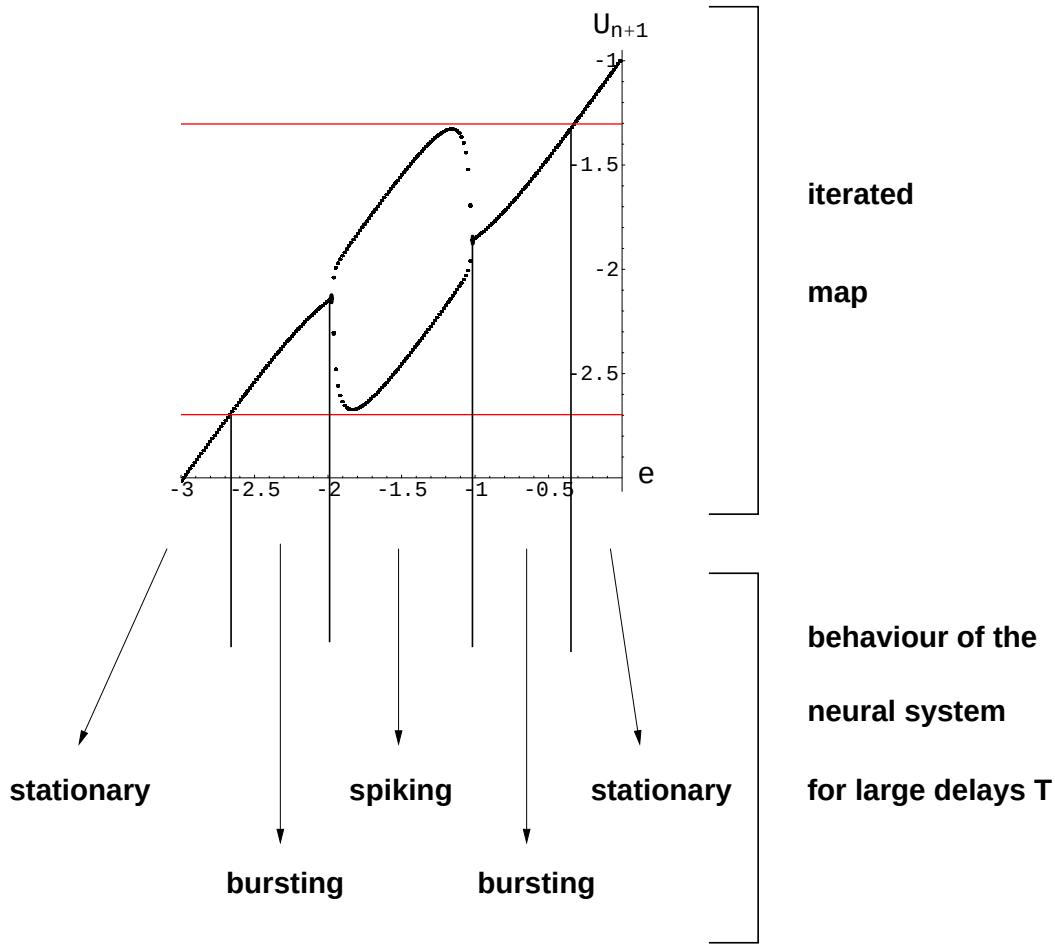

Figure 9.3: Zuordnung von Bereichen des Verzweigungsdiagramms der iterierten Abbildung zum Verhalten des Neuronenmodells für große Zeitverzögerungen.

- Für große/unendliche Zeitverzögerungen: Bursting tritt für solche Parameterwerte e auf, die einer stationären Lösung der iterierten Abbildung entsprechen, wobei diese stationäre Lösung im Oszillationsintervall des FitzHugh-Nagumo Oszillators liegen muss. Spiking entspricht dann Parameterwerten e, für die die iterierte Abbildung periodische Lösungen besitzt (siehe Abbildung 9.3).
- Für endliche/kleine Zeitverzögerungen: Bursting tritt für Parameterwerte e auf, die instabilen Bereichen auf dem Zweig der periodischen Lösung entsprechen. Stabile Bereiche des Zweiges der periodischen Lösung entsprechen Spiking.

9.1.4 Systeme mit vielen Zeitskalen

Die Untersuchungen der Dissertation werden durch ein Anwendungsbeispiel für Bursting abgeschlossen. In der Natur treten viele Arten postsynaptischer Potentiale auf, die in die Basiskategorien schnell, langsam, inhibitorisch und exzitatorisch eingeteilt werden können. Durch die Hinzunahme weiterer Netzgleichungen in das Modell wurde es möglich, diese Klassen postsynaptischer Potentiale für ein kleines neuronales Netz von drei Neuronen zu modellieren (siehe Abbildung 9.4).

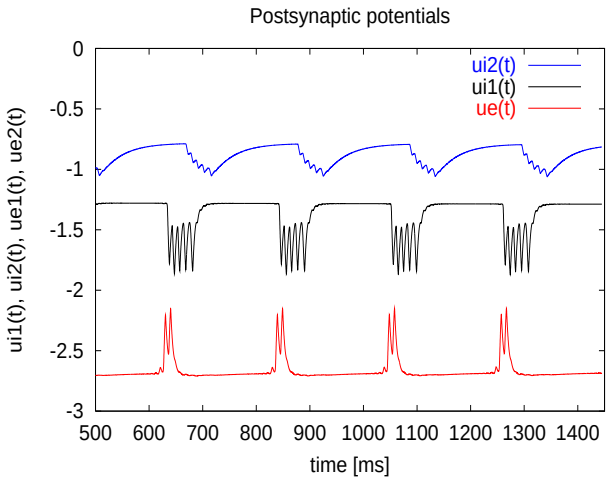

Figure 9.4: Modellierung verschiedener postsynaptischer Potentiale. Das blaue Potential (ui2) entspricht einem langsamen inhibitorischen postsynaptischen Potential, das schwarze Potential (ui1) einem schnellen inhibitorischen postsynaptischen Potential und das rote Potential (ue=ue1=ue2) ist ein schnelles exzitatorisches postsynaptisches Potential.

Das neuronale Netz zur Modellierung postsynaptischer Potentiale weist eine interessante Eigenschaft auf: Mit wachsender Zeitverzögerung zeigen die Potentiale die Bildung von Burst-Multipletts (siehe Abbildung 9.5). Dies sind Einheiten einer gewissen Anzahl von Bursts, die sich periodisch wiederholen. Um eine numerische Analyse des Burstverhaltens durchführen zu können, wird das Modell auf ein System mit nur noch drei Zeitskalen reduziert, ohne dass das Auftreten von Burst-Multipletts verloren geht.

$$\begin{aligned} \tau\dot{u}(t) &= -u(t) + q\{g(v(t)) + g(v(t-T))\} + e, \\ \dot{v}(t) &= c(w(t) + v(t) - \frac{1}{3}v^3(t)) + \gamma u(t), \\ \dot{w}(t) &= (a - v(t) - bw(t))/c. \end{aligned}$$

Die Analyse dieses Systems zeigt, dass es zwischen den Zuständen mit Burst-Multipletts Übergangsphasen gibt, die ein eher chaotisches Verhalten zeigen. Es

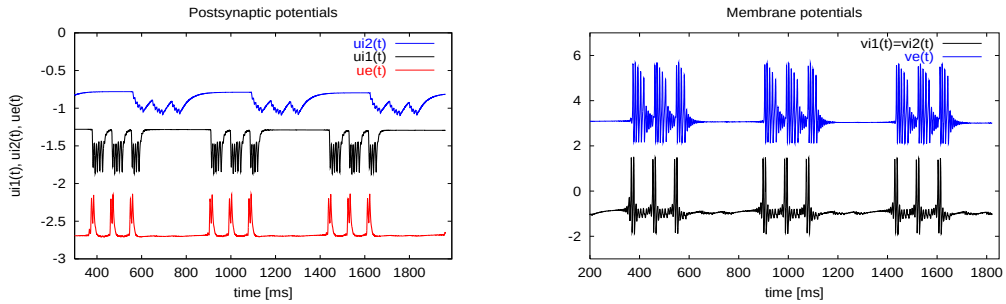

Figure 9.5: Burst-Multipletts des postsynaptischen Potentials und des Membranpotentials in einem kleinen neuronalen Netz.

wird auch beobachtet, dass die Dynamik der Burst-Multipletts mit wachsender Anzahl der Bursts ebenfalls komplexer wird.
Burst-Multipletts treten auch in realen neuronalen Netzen auf; sie wurden zum Beispiel im Hirnstamm der Kaulquappe nachgewiesen.

Appendix A

Hodgkin-Huxley equations

The Hodgkin-Huxley model was developed in order to describe the action potentials in the squid giant axon. v denotes the membrane potential of the cell and the variables m, n and h describe the conductance of the cell membrane for different types of ions (sodium, potassium and the rest is summed in a leak term).

$$\begin{aligned} C_m \frac{dv}{dt} &= -\bar{g}_K n^4 (v - v_K) - \bar{g}_{Na} m^3 h (v - v_{Na}) - \bar{g}_L (v - v_L) + I_{app}, \\ \frac{dm}{dt} &= \alpha_m (1 - m) - \beta_m m, \\ \frac{dn}{dt} &= \alpha_n (1 - n) - \beta_n n, \\ \frac{dh}{dt} &= \alpha_h (1 - h) - \beta_h h. \end{aligned}$$

The specific functions α and β depend on the membrane potentials and it holds

$$\begin{aligned} \alpha_m(v) &= 0.1 \, \frac{25 - v}{\exp\left(\frac{25-v}{10}\right) - 1}, \\ \beta_m(v) &= 4 \, \exp\left(\frac{-v}{18}\right), \\ \alpha_h(v) &= 0.07 \, \exp\left(\frac{-v}{20}\right), \\ \beta_h(v) &= \frac{1}{\exp\left(\frac{30-v}{10}\right) + 1}, \\ \alpha_n(v) &= 0.01 \, \frac{10 - v}{\exp\left(\frac{10-v}{10}\right) - 1}, \\ \beta_m(v) &= 0.125 \, \exp\left(\frac{-v}{80}\right). \end{aligned}$$

The conductivity parameters are $\bar{g}_{Na} = 120$, $\bar{g}_K = 36$ and $\bar{g}_L = 0.3$. For the equilibrium potentials holds $v_{Na} = 115$, $v_K = -12$ and $v_L = 10.6$.
A detailed review of the properties of the Hodgkin-Huxley model is given in [25].

Appendix B

Inverse function $H^{-1}(U(s))$

Starting out from the limiting case $T \to \infty$ the neural system is described by a difference-algebraic system

$$\begin{aligned} 0 &= -U(s) + qg(V(s-1)) + e, \\ 0 &= c(W(s) + V(s) - \frac{1}{3}V^3(s)) + U(s), \\ 0 &= (a - V(s) - bW(s))/c \end{aligned}$$

with an auxiliary function

$$H(V(s)) := c(\frac{1}{3}V^3(s) + V(s)(\frac{1}{b} - 1) - \frac{a}{b}) = U(s).$$

The inverse of $H(V(s))$ is

$$H^{-1}(U(s)) = \frac{-3\,2^{\frac{1}{3}}\,(-c + b\,c)}{\left(-81\,a\,b^2\,c^3 - 81\,b^3\,c^2\,u + \sqrt{-2916\,b^3\,c^3\,(-c + b\,c)^3 + (-81\,a\,b^2\,c^3 - 81\,b^3\,c^2\,u)^2}\right)^{\frac{1}{3}}}$$

$$- \frac{\left(-81\,a\,b^2\,c^3 - 81\,b^3\,c^2\,u + \sqrt{-2916\,b^3\,c^3\,(-c + b\,c)^3 + (-81\,a\,b^2\,c^3 - 81\,b^3\,c^2\,u)^2}\right)^{\frac{1}{3}}}{3\,2^{\frac{1}{3}}\,b\,c}.$$

Bibliography

[1] U. an der Heiden. *Analysis of neural networks*, volume 35 of *Lecture Notes in Biomathematics*. Springer-Verlag, Berlin, 1980.

[2] S. Bernard, J. Bélair, and M. Mackey. Oscillations on cyclical neutropenia: new evidence based on mathematical modeling. *J. Theoretical Biology*, 223:283–298, 2003.

[3] R. J. Butera, Jr., J. Rinzel, and J. C. Smith. Models of Respiratory Rhythm Generation in the Pre-Bötzinger Complex. II. Populations of Coupled Pacemaker Neurons. *J. Neurophysiol.*, 82:398–415, 1999.

[4] A. Destexhe, D. A. McCormick, and T. J. Sejnowski. A model for 8-10 Hz spindling in interconnected thalamic relay and reticularis neurons. *Biophys. J.*, 65:2474–8, 1993.

[5] A. Destexhe and T. J. Sejnowski. *Thalamocortical Assemblies.* Oxford University Press, New York, 2001.

[6] O. Diekmann, S. A. van Gils, S. M. Verduyn Lunel, and H.-O. Walther. *Delay equations*, volume 110 of *Applied Mathematical Sciences*. Springer-Verlag, New York, 1995. Functional, complex, and nonlinear analysis.

[7] E. J. Doedel, A. R. Champneys, T. F. Fairgrieve, Y. A. Kuznetsov, B. Sandstede, and X.-J. Wang. AUTO97: Continuation and bifurcation software for ordinary differential equations. Technical report, Department of Computer Science, Concordia University, Montreal, Canada, 1997. (Available by FTP from ftp.cs.concordia.ca in directory pub/doedel/auto).

[8] R. D. Driver. *Ordinary and delay differential equations.* Springer-Verlag, New York, 1977. Applied Mathematical Sciences, Vol. 20.

[9] K. Engelborghs, L. Luzyanina, and G. Samaey. DDE-BIFTOOL v. 2.00: a Matlab package for bifurcation analysis of delay differential equations. Technical Report TW-330, Department of Computer Science, K.U. Leuven, Leuven, Belgium, 2001.

[10] B. Ermentrout. *XPPAUT 5.5 - the differential equations tool.* Available from http://www.math.pitt.edu/ bard/xpp/download. html.

[11] C. P. Fall, E. S. Marland, J. M. Wagner, and J. J. Tyson, editors. *Computational cell biology*, volume 20 of *Interdisciplinary Applied Mathematics.* Springer-Verlag, New York, 2002.

[12] R. FitzHugh. Impulses and physiological states in theoretical models of nerve membrane. *Biophysical Journal*, 1:445–466, 1961.

[13] F. Giannakopoulos, U. Bihler, C. Hauptmann, and H. J. Luhmann. Epileptiform activity in a neocortical network: a mathematical model. *Biological Cybernetics*, 85:257–268, 2001.

[14] F. Giannakopoulos, C. Hauptmann, and A. Zapp. Bursting activity in a model of a neuron with recurrent synaptic feedback. In *Topics in functional differential and difference equations (Lisbon, 1999)*, volume 29 of *Fields Inst. Commun.*, pages 147–159. Amer. Math. Soc., Providence, RI, 2001.

[15] K. Green and B. Krauskopf. Bifurcation analysis of frequency locking in a semiconductor laser with phase conjugate feedback. *Int. J. Bifurcation and Chaos*, 13(9):2589–2601, 2003.

[16] J. Guckenheimer and P. Holmes. *Nonlinear oscillations, dynamical systems, and bifurcations of vector fields*, volume 42 of *Applied Mathematical Sciences.* Springer-Verlag, New York, 1990. Revised and corrected reprint of the 1983 original.

[17] K. P. Hadeler, U. an der Heiden, and K. Schumacher. Generation of the nervous impulse and periodic oscillations. *Biol. Cybernet.*, 23(4):211–218, 1976.

[18] J. K. Hale and H. Koçak. *Dynamics and bifurcations*, volume 3 of *Texts in Applied Mathematics.* Springer-Verlag, New York, 1991.

[19] J. K. Hale and S. M. Verduyn Lunel. *Introduction to functional-differential equations*, volume 99 of *Applied Mathematical Sciences.* Springer-Verlag, New York, 1993.

[20] C. Hauptmann. *Epileptiform activity in differential equation models of neuronal networks.* Shaker Verlag, Aachen, 2000.

[21] C. Hauptmann, A. Gail, and F. Giannakopoulos. Intermittent burst synchronization in neural networks. *Lecture Notes in Computer Science*, 2686:46–53, 2003.

[22] T. Heil, I. Fischer, B. Elsäßer, B. Krauskopf, K. Grenn, and A. Gavrielides. Delay dynamics of semiconductor lasers with short external cavities: bifurcation scenarios and mechanisms. *Physical Review E*, 67(6):1–11, 2003.

[23] A. Hodgkin and A. Huxley. A quantitative description of membrane current and application to conduction and excitation. *J. Physiol.*, 117:500–544, 1952.

[24] E. Kaumann and U. Staude. Uniqueness and nonexistence of limit cycles for the Fitz Hugh equation. In H. W. Knobloch and K. Schmitt, editors, *Equadiff 82. Lecture notes in mathematics.*, volume 1017, pages 313–321. Springer Verlag, Berlin, 1983.

[25] J. Keener and J. Sneyd. *Mathematical physiology*, volume 8 of *Interdisciplinary Applied Mathematics*. Springer-Verlag, New York, 1998.

[26] B. Krauskopf. Bifurcation analysis of lasers with delay. In D. Kane and K. Shore, editors, *Unlocking Dynamical Diversity: Optical Feedback Effects on Semiconductor Lasers*. Wiley, to appear.

[27] B. Krauskopf and K. Green. Computing unstable manifolds of periodic orbits in delay differential equations. *J. Computational Physics*, 186(1):230–249, 2003.

[28] Y. A. Kuznetsov. *Elements of applied bifurcation theory*, volume 112 of *Applied Mathematical Sciences*. Springer-Verlag, New York, second edition, 1998.

[29] J. Nagumo, S. Arimoto, and S. Yoshizawa. An active pulse transmission line simulating nerve axon. *Proc. IRE*, 50:2061–2070, 1964.

[30] L. G. Nowak, M. Azouz, R. amd Sanchez-Vives, C. Gray, and D. McCormick. Electrophysiological Classes of Cat Primary Visual Cortical Neurons In Vivo as Revealed by Quantitative Analyses. *J. Neurophysiol.*, 89:1541–1566, 2003.

[31] G. M. Shepherd. *The synaptic organization of the brain*. Oxford University Press, New York, 3rd edition, 1990.

[32] A. Shilnikov, R. Calabrese, and G. Cymbalyuk. Mechanisms of bi-stability: tonic spiking and bursting in a neuron model. *Submitted to Phys.Review E*.

[33] M. Steriade, D. A. McCormick, and T. J. Sejnowski. Thalamocortical Oscillations in the Sleeping and Aroused Brain. *Science*, 262:679–685, 1993.

[34] C. Torgerson, M. Gdovin, and J. E. Remmers. Fictive gill and lung ventilation in the pre- and postmetamorphic tadpole brain stem. *J. Neurophysiol.*, 80:2022–2025, 1998.

[35] W. Troy. Bifurcation phenomena in FitzHugh's nerve conduction equation. *J. Math. Annal. Appl.*, 54:678–690, 1976.

[36] S. Wiggins. *Introduction to applied nonlinear dynamical systems and chaos*, volume 2 of *Texts in Applied Mathematics*. Springer-Verlag, New York, 1990.

List of Figures

Acknowledgements

I would like to thank Prof. Dr. Tassilo Küpper and Prof. Dr. Dietrich Stauffer who enabled this Ph.D. thesis and supported my work.

I am grateful to PD Dr. Fotios Giannakopoulos for his interest and help with regard to the scientific content and the progress of this thesis.

My thanks also comprise Mrs. Marion Adam and my colleagues for their advice and the good working atmosphere at the Mathematical Institute.

Finally, I would like to thank the *Deutsche Forschungsgemeinschaft* for funding me within the Graduiertenkolleg *Scientific Computing* at the University of Cologne.

Ich versichere, daß ich die von mir vorgelegte Dissertation selbständig angefertigt, die benutzten Quellen und Hilfsmittel vollständig angegeben und die Stellen der Arbeit - einschließlich Tabellen, Karten und Abbildungen -, die anderen Werken im Wortlaut oder dem Sinn nach entnommen sind, in jedem Einzelfall als Entlehnung kenntlich gemacht habe; daß diese Dissertation noch keiner anderen Fakultät oder Universität zur Prüfung vorgelegen hat; daß sie abgesehen von unten angegebenen Teilpublikationen noch nicht veröffentlicht worden ist sowie, daß ich eine solche Veröffentlichung vor Abschluß des Promotionsverfahrens nicht vornehmen werde. Die Bestimmungen dieser Promotionsordung sind mir bekannt. Die von mir vorgelegte Dissertation ist von Prof. Dr. Tassilo Küpper betreut worden.

Teilpublikation: C. Hauptmann, A. Gail, F. Giannakopoulos,
Intermittent Burst Synchronization in Neural Networks,
Lecture Notes in Computer Science 2686, p. 46-53, 2003.

Bursting in a model with delay for networks of neurons

It is the intention of this thesis to analyse the mechanisms that lead to bursting in a neuron model. The neuron model used within the thesis describes the membrane potentials as well as the postsynaptic potentials of neurons. The neuron is modelled by a coupled nonlinear system of three differential equations with delay. It consists of a FitzHugh-Nagumo oscillator that is to be considered as an oscillation generator at the axon hillock of the neuron. Further, the model consists of a network equation that sums up all incoming signals and describes the synaptic properties of the neuron. The solutions of the neuron model display three different types of dynamics: stationary behaviour, bursting and spiking. Bursting is characterised by periodic oscillations that are separated by phases of quasistationary behaviour. Permanent oscillations however are called spiking. The different types of dynamics depend on the parameters of the neuron model. Bursting in the analysed model has been regarded up to now as a phenomenon that arises due to the interaction of different time scales within the model. Parameter values that lead to bursting were obtained empirically.
It was the aim of this thesis to find a connection between the appearance of bursting and the bifurcation properties of the neuron model.
For this purpose the neuron model was analysed using three different approaches. These were the analysis of the complete system for the limiting case of infinite delay time T of the model, the analysis of the stability of the stationary solutions of the model for finite and infinite delay and a bifurcation analysis of the complete system using a numerical bifurcation tool for delay differential equations. The investigations resulted in criteria for the occurence of bursting with respect to the bifurcation parameter for small/finite and large/infinite delay. Finally in this thesis the neuron model was used to describe qualitatively the behaviour of postsynaptic potentials of nerve cells. The idea of different time scales was applied to a small but realistic neural network of three neurons which made it possible to model different types of postsynaptic potentials.

Bursting in Modellen mit Zeitverzögerung für neuronale Netze

In der vorliegenden Arbeit werden Mechanismen, die zu Bursting in einem Neuronenmodell führen, untersucht. Als Bursting wird eine Oszillationsform der Potentiale von Nervenzellen bezeichnet, die sich durch Phasen periodischer Aktivität auszeichnet. Zwischen den Phasen periodischer Aktivität zeigt sich quasistationäres Verhalten. Eine weitere Oszillationsart von Nervenzellen ist Spiking, das ein kontinuierliches Oszillieren des Potentials bezeichnet.
In bisherigen Veröffentlichungen zu dem verwendeten Neuronenmodell wurden für das Auftreten von Bursting empirisch gefundene Kriterien angegeben. Das heißt, dass aus numerischen Simulationen Parameterbereiche abgeleitet wurden, für die Bursting auftritt. Ziel dieser Arbeit ist es, Kriterien für das Auftreten von Bursting zu finden, die sich direkt aus den Verzweigungseigenschaften des Modells herleiten lassen.
Das Neuronenmodell, das in dieser Arbeit untersucht wird, besteht aus drei gekoppelten nichtlinearen Differentialgleichungen mit Zeitverzögerung.
Um Kriterien für das Auftreten von Bursting zu finden, die auf der Parameterabhängigkeit des Modells beruhen, müssen die Verzweigungseigenschaften des neuronalen Systems untersucht werden. Dies wurde in der Arbeit mittels drei verschiedener Ansätze durchgeführt: Die Untersuchung des Systems im Fall unendlicher Zeitverzögerung, die Analyse der Stabilität der stationären Lösungen für endliche und unendliche Zeitverzögerung sowie eine numerische Bifurkationsanalyse des Systems. Die Kombination der Ergebnisse dieser Ansätze ermöglicht es dann, Bedingungen anzugeben, für die Bursting in Abhängigkeit vom Verzweigungsparameter auftritt.
Die Untersuchungen der Dissertation werden durch ein Anwendungsbeispiel für Bursting abgeschlossen. In der Natur treten viele Arten postsynaptischer Potentiale auf, die in die Basiskategorien schnell, langsam, inhibitorisch und exzitatorisch eingeteilt werden können. Durch die Hinzunahme weiterer Netzgleichungen in das Modell wurde es möglich, diese Klassen postsynaptischer Potentiale für ein kleines neuronales Netz zu modellieren.